Mathematical Modelling of Size Exclusion Chromatography of Polymers

By

Gregory Afacan

A thesis submitted in partial fulfillment of the requirements for the degree of

Master of Science

in

Chemical Engineering

Department of Chemical and Materials Engineering

University of Alberta

Abstract

Size-exclusion chromatography (SEC) is a valuable liquid chromatography tool for the analytical or preparative fractionation of proteins and polymers. SEC separates macromolecules according to differences in their hydrodynamic volumes. It does not rely on any binding between the solutes and the stationary phase. As the solutes travel through a packed SEC column, larger molecules are less prone to entering the pores of the stationary phase and thus have shorter retention times. Smaller molecules permeate more deeply into the pores of the stationary phase, thus delaying their elution as they spend more time in the column. In early design stages, it is practical to simulate liquid chromatography processes using rate models. This cuts costs and time associated with physical experiments and mitigates any errors when relying on trial and error methods for scale-up. In this work, two mathematical models of the SEC process have been developed. The first is a predictive model that generates separate elution profiles for various molecular weights contained within a specified molecular weight distribution (MWD), which can be described by the Poisson distribution. These elution profiles resemble a Gaussian distribution, and added together, form the final chromatographic profile. The second method is a mathematical rate model considering various mass transfer effects using a lumped kinetic model where all sources of mass transport resistances were combined into the mass transfer coefficient. As an experimental base for the analysis, 12 polystyrene standards of varying molecular weights were selected. The experiments were performed using three linear columns (PLgel Olexis, 13 μm gel particles, and 300 mm × 7.5 mm) at 145 °C. 200 microliters of a polymer solution were injected into the columns at a flow rate of 1.0 mL/min of trichlorobenzene (TCB). The accuracy of each model was verified by comparing the predicted and simulated results to the experimental data. Both models accurately predicted the retention times and peak shapes of unimodal and multimodal polystyrene standard samples.

Preface

Two mathematical models of the size-exclusion chromatography process were developed for the purposes of scale-up. The first was a predictive model implementing Poisson and Gaussian distributions, and the second was a simplified version of the general rate model.

Chapter 1 gives a brief history of the size-exclusion process and reviews how polymer properties are measured and how they affect polymer end uses. Present day scale-up procedures and their drawbacks are also defined in this chapter.

Chapter 2 reviews the previous scientific literature on size-exclusion chromatography. This chapter describes the separation mechanism, as well as essential chromatography concepts such as: molecular weight distribution, polydispersity, retention, and efficiency. The importance of band broadening is also defined in this chapter.

Chapter 3 details the type of column and polystyrene standards used in this investigation. It also details the methodology used to develop each mathematical model. The predictive model originates from the Poisson distribution that describes the molecular weight distribution of a specific polymer. The simplified general rate model was derived by performing mass balances on a section of the size-exclusion chromatography column. Differential equations of the rate model were solved using the finite volume method.

Chapter 4 compares simulated and experimental results for unimodal and multimodal polystyrene standard samples. This chapter discusses the agreement between the simulated and experimental results.

Chapter 5 proposes the main conclusions of this study and suggests future research work. The results from *Chapter 4* are summarized and suggestions for future studies to strengthen key knowledge gaps are also provided.

Acknowledgments

I would like to thank Dr. João B. P. Soares for the opportunity to work under his supervision. Without his indispensable guidance and support, this thesis would not have been possible. His passion, knowledge, and attitude are inspirational, and I hope to become half the chemical engineer he is right now.

I would also like to offer my deepest appreciation for my co-supervisor Dr. Arvind Rajendran. Thank you for challenging me and encouraging me to challenge myself. I am completely indebted to Arvind for the academic and life lessons he taught me throughout the course of my research. Most importantly, thank you for your patience with me.

Additionally, thank you to the members of Arvind's group Nick, Gokul, and Nagesh. I am grateful for your assistance, knowledge, experience, and friendship.

I also want to acknowledge the current and past members of the Group of Applied Macromolecular Engineering. They have not only been wonderful colleagues but also amazing friends.

A special thanks are owed to my parents and sister for their love and support. Thank you for teaching me the value of hard work and dedication. I would also like to thank my girlfriend, Cristina, for her encouragement and believing in me.

Finally, thank you to my brother Chris. Life is made easier with you in it.

Table of Contents

List of Figures

List of Tables

Chapter 1 Introduction

1.1 History of the Chromatographic Process

In the early 1900s, Mikhail Tswett showed that plant extracts could be fractionated through his invention of classical column chromatography [1]. It was developed in a time when the acquisition of physio-chemical data was slow and limited to parameters of low specificity [2]. Chromatography is a separation process based on the difference between migration velocities of the distinct components in a mixture, as it travels through a bed of solid or porous particles contained in a column [3]. There are three possible forms of chromatography, which can be classified according to the fluid used as the mobile phase. The fluid can be a liquid, a gas, or a supercritical fluid. High performance liquid chromatography (HPLC) represents the culmination of developments in liquid chromatography. There are many types of HPLC, such as reversed-phase chromatography, ion-exchange chromatography, and size-exclusion chromatography (SEC). Modern, high-performance SEC is a result of the development of small, more rigid porous particles for column packings [4].

1.2 Size-Exclusion Chromatography

Size-exclusion chromatography constitutes a major portion of commercial chromatographic processes and purifications. Introduced in 1964 [5], SEC has proven to be a vital tool for the analysis and separation of macromolecules such as proteins and polymers [6]. The principle use of SEC is determining the molecular weight distributions and averages of natural and synthetic polymers [4]. This is achieved through the separation of molecules according to their hydrodynamic volumes. Smaller molecules enter the pores of the packing, are trapped and removed from the main flow of the mobile phase. Molecules that are larger than the average pore size of the porous packing are excluded from the pores, and thus suffer essentially no retention.

The properties and applications of polymers are determined by their chemical and physical distributions [7]. Table 1.1 lists the types of separation methods used for measuring these distributions. SEC-based methods make up the majority of techniques used. Combining SEC with other analytical techniques such as light scattering, viscometry, and mass spectroscopy only strengthens its analytical ability.

Table 1.1: Macromolecular distributions: their measurement and end-use effects. Modified from Striegal et al. [7].

Macromolecular Property	Properties Affected	Separation Method Used for Determination[a]
Molar mass	Elongation, tensile strength, adhesion	SEC, FFF, HDC, TGIC, CEC, SFC,
Long-chain branching	Shear strength, tack, peel, crystallinity	SEC-MALLS, SEC-VISC
Short-chain branching	Haze, stress-crack resistance, crystallinity	SEC-IR, SEC-NMR, TREF, CRYSTAF
Cross-linking	Gelation, vulcanization, surface roughness	SEC-MALLS, SEC-VISC
Tacticity	Crystallinity, anisotropy, solubility	SEC-NMR, TGIC, LCCC
Chemical heterogeneity	Toughness, brittleness, biodegradability	SEC-spectroscopy, LCCC
Chemical composition vs. molar mass	Mechanical properties, blending, plasticization	SEC-GPEC

[a]*SEC* size exclusion chromatography, *FFF* field flow fractionation, *HDC* hydrodynamic chromatography, *TGIC* temperature gradient interaction chromatography, *CEC* capillary electrokinetic chromatography, *SFC* supercritical fluid chromatography, *LCCC* liquid chromatography at critical conditions, *MALLS* multi-angle laser light scattering, *VISC* viscometry, *TREF* temperature rising elution fractionation, *CRYSTAF* crystallization fractionation, *GPEC* gradient polymer elution chromatography

1.3 Modeling and Scalability

General scale-up rules are used in conjunction with trial and error procedures for SEC. More specifically, empirical/semi-empirical relationships relating particle size, flow rate, and column length rely on rule of thumbs for scale-up. Instead, rate models can be used to simulate chromatograms of small and large columns before they are built or purchased. Scalability models use experimental data obtained from a bench scale column with the same packing as a large column. As a result, rate models and simulation potentially provide a more accurate scale-up of liquid chromatography system than current practices.

1.4 Problem Statement

HPLC is considered the leading technique for chemical analysis [8]. It has become increasingly popular due to its ability to separate, purify, and analyze at preparative and large scales. However, large scale LC columns suffer from lower performances due to dispersion effects when compared to small scale analytical HPLC, which exhibit near plug flow results [8]. Design and scale-up of liquid chromatography was largely empirical [9] and relied on trial and error in combination with estimating mass transfer parameters using existing correlations. Recently, more advanced modelling tools are being used to scale up HPLC. However, an incorrect estimation will negatively affect performance, resulting in insufficient resolution. Therefore, an appropriate mathematical model is important for optimal analysis of separation and scalability. Establishing an accurate scale-up method will allow the application of experimental data to support the use of SEC beyond small-scale operations for preparative purification of biomolecules and preparative fractionation of polymers using columns.

1.5 Objectives

This research work tested whether it was possible to mathematically model size-exclusion chromatography for the purposes of scale-up.

The specific objectives of this study are:

I. Develop a model for the size-exclusion chromatography process for various polystyrene standards.
II. Investigate the validity of the model by comparing the simulated results with experimental data.

Chapter 2 Literature Review

2.1 Introduction

Separation and purifications are essential in many industrial processes pertaining to medical, chemical, environmental, and pharmaceutical technologies. Listed below are several of the most commonly used modes of interaction related to the design of preparative separations used in industry:

1. *Ion-exchange chromatography*

   Ion-exchange chromatography (IEC) is the most widely used mode of chromatography for protein separation. Separation takes place because of differential ionic interactions between the stationary phase and feed [10]. Components are eluted in order of increasing binding strength with the stationary phase.

2. *Hydrophobic interaction chromatography*

   Hydrophobic interaction chromatography (HIC) has become a popular technique for the separation of biological compounds where solutes are adsorbed to a neutral or mildly hydrophobic stationary phase. Solutes are then eluted in the order of increasing surface hydrophobicity as the salt concentration of the mobile phase is decreased, causing desorption [11].

3. *Reversed-phase chromatography*

   Similar to HIC, reversed-phase chromatography is based on the differences in the hydrophobicities of the different sample components [12]. Polar compounds travel faster and are eluted first due to a lesser affinity to the non-polar stationary phase, that is, the more nonpolar the component is, the longer it will be retained in the column.

4. *Affinity chromatography*

   Affinity chromatography makes use of specific binding interactions between molecules. Biological macromolecules interact with other molecules with high specificity through hydrogen bonding, ionic and hydrophobic interactions, and other specific interactions [10]. As a result, this technique provides high selectivity and high resolution.

2.2 Scale-Up in Liquid Chromatography

A typical scale-up from lab scale to pilot plant is in the order of 50-100-fold, while a scale-up from a pilot plant to final commercial scale is in the order of 10-50-fold [10, 11]. The usual basis for the scale-up of separation processes is to keep the plate count constant and proportionally increase the feed volume and column dimensions.

Rathore and Velayudhan [11] outlined several issues that must be considered when attempting to scale up a separation process:

1. *Bed stability (physical)*

   On a laboratory scale, the column wall offers significant support to the column bed. When a column is scaled up, its diameter increases, which causes the wall support contribution to bed stability to decrease. This could result in the redistribution of particles and settling of the bed.

2. *Bed stability (chemical)*

   Chemical stability of the stationary phase is dependent on any factors resulting in the deterioration of the packing material. This issue becomes more significant when the column is reused many times during commercial processing.

3. *Product loading*

   During scale-up, product loading is commonly held constant. However, column resolution can decrease if the loading reaches a certain level.

4. *Gradient separations*

   As the scale of the processes increases, buffer volumes also increase, making it more difficult to obtain accurate and reproducible gradients.

5. *Flow distributions*

   On a laboratory scale, a uniform flow distribution at the column head is easily achieved, however this becomes more difficult as the diameter of the column increases. This may result in deviations from plug flow, leading to peak tailing.

6. *Packing quality*

   To obtain uniform flow distribution, homogenous packing is critical to avoid channelling. However, it can sometimes be difficult to achieve homogeneity when packing large columns.

7. *System design*

   Contributions to dead volume from valves, flow meters, air sensors, tubing, piping, and other support equipment is much larger at an industrial scale than in a lab scale system. This leads to higher pressure drops as well as additional band broadening, which impacts the overall column performance.

8. *Fraction collection*

   Peak width and shape shown in the chromatogram depends on column dimensions, extra-column effects, operating conditions, and sample volume. Therefore, it is likely that peak width and shape may be different compared to the lab scale results. The fraction collection method should be studied based on the column performance at the final scale.

9. *Costing*

   The cost of the feedstock should be given significant consideration when process is scaled up. When the process is modeled on a large scale, the raw materials and facility costs must be examined.

10. *Sample pre-treatment*

    Pre-treatment of the process stream at large scale to remove all harmful impurities is important to maintain desired column performance.

Currently, trial and error and general correlations are used for the scale-up of liquid chromatography [12], but these methods are not necessarily accurate or reliable. From Snyder and Kirkland [13], along with others [2, 14], it can be seen that these correlations are mostly empirical or semiempirical relationships about particle size, flow rate, column length, and resolution.

As an alternative to following these scale-up rules, rate models can be used to simulate chromatograms of a large-scale column before it is built. Experimental data obtained from a small

column with the same packing as the large column is used to generate the chromatograms in an inexpensive manner.

2.3 Introduction to Size-Exclusion Chromatography

A schematic of the SEC process is shown in Figure 2.1. As discussed previously, size-exclusion chromatography separates a mixture according to the size of the species in solution, i.e. the hydrodynamic volume, rather than by enthalpic interactions with the solid phase. The SEC column is packed with porous beads of predefined porosity and particle size. The species is prepared as a dilute solution in the eluent and injected into the system. As shown in Figure 2.2, molecules larger than the accessible particle porosity are not able to permeate (total exclusion limit) the pores, while small molecules can permeate more deeply into the solid phase (total permeation limit) [10]. This means larger size molecules are eluted first, followed by the smaller ones. In the characterization of polymers, the elution time or volume can then be correlated to a molar mass which is dependent on the type of polymer. The species can have a diverse range of physical properties, whether it is a single molecule, an aggregate, a micelle, or a polymer coil [15]. Consequently, the aggregation phenomena in solution, as well as the molar mass distribution of the polymer, can be studied using SEC. Typically, SEC is applied to the analysis of synthetic polymers and oligomers [15-17], coal-derived substances [18,19], lipids [20,21], and natural macromolecules such as proteins [22-24].

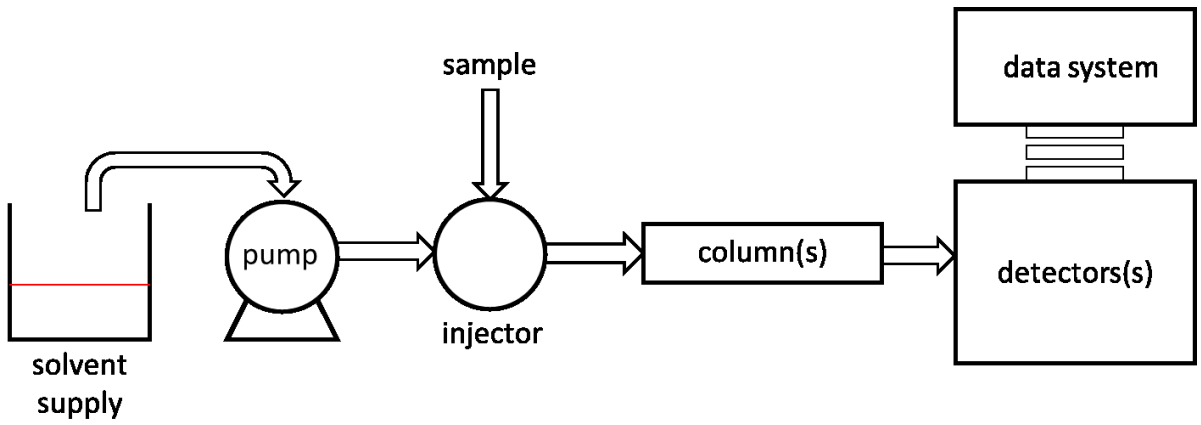

Figure 2.1: Schematic of a typical SEC instrument.

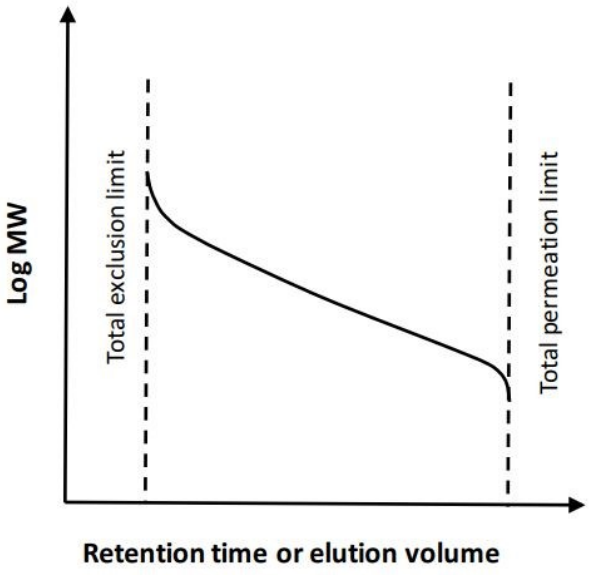

Figure 2.2: Relationship between molecular weight and retention time [8].

2.4 Separation Mechanism of SEC

The driving force in size-exclusion chromatography is the concentration gradient between stationary and mobile phases [4,25]. This is due to the solute bands repeatedly permeating in and out of the porous particles as the band travels along with the solvent down the column. Intuitively, no fraction of the sample can be eluted before the volume of the solvent outside the particles has passed the column. This is known as the interstitial volume, V_i, and corresponds to the exclusion limit of the column. Molecules with the ability to diffuse into the entire volume of the pores, V_p, will elute at a volume equal to the sum of the interstitial volume, V_i, and the pore volume V_p [26]. Therefore, molecules eluted at a volume in between these extremes, V_e, have access to only a fraction of the pore volume as shown by the expression

$$V_e = V_i + K_{SEC}V_p \tag{2.1}$$

where K_{SEC} is the SEC distribution coefficient. K_{SEC} is a thermodynamic parameter that can be defined as the ratio of the average concentration, $\langle c \rangle$, of the solute in the pore volume to that in the interstitial volume [27]

$$K_{SEC} = \frac{\langle c \rangle_p}{\langle c \rangle_i} \tag{2.2}$$

The coefficient K_{SEC} varies from 0 and 1. If K_{SEC}> 1, the separation is controlled by enthalpic interactions, which depend on the chemical compositions of solute and stationary phases, and not necessarily on the molecular weight of the solute.

2.5 Size-Exclusion Chromatography Thermodynamics

As previously stated, solute molecules continually transfer between interstitial and pore volumes, redistributing themselves between phases to satisfy thermodynamic equilibrium. Thermodynamic equilibrium is reached when the chemical potential of each solute component is the same in the mobile and stationary phases [28]. At constant temperature and pressure, the Gibbs free-energy difference, ΔG, between the phases can describe the solute distribution at equilibrium [29]

$$\Delta G = \Delta H - T\Delta S = -RT \ln K \tag{2.3}$$

where R is the gas constant and T is the absolute temperature. ΔH is the change in enthalpy and ΔS is the change in entropy when a mole of solute is transferred from the interstitial to the pore volume under standard conditions. Rearranging Equation (2.3) to solve for the distribution coefficient as a function of $1/T$ yields

$$K = e^{-\frac{\Delta H}{RT} + \frac{\Delta S}{R}} \tag{2.4}$$

Most forms of liquid chromatography depend on substantial enthalpy changes and intermolecular forces, such as absorption or adsorption [25,29]. Assuming the entropy change is negligible, one can write Equation (2.4) as

$$K_{LC} \cong e^{-\frac{\Delta H}{RT}} \tag{2.5}$$

The attractive solute-stationary phase interaction is usually exothermic. As a result, the value for ΔH will be negative, resulting in K_{LC} to be larger than 1. However, pure size exclusion separation

is controlled mainly by the entropy change between phases [30,31]. Since enthalpy change is negligible, one may derive K_{SEC} using Equation (2.4) as

$$K_{SEC} \cong e^{\frac{\Delta S}{R}} \tag{2.6}$$

Therefore, the value of K_{SEC} is proportional to the decrease in entropy experienced as the polymer chains diffuse into the pores of the packing, as represented in Figure 2.3. In panel A, the solute elutes later as it is able to permeate the entire volume of the porous material resulting in no substantial change in entropy. In panel B, the solute can only occupy a finite volume of the pores; entropy is negative and K_{SEC} decreases. Finally, panel C shows the solute elutes sooner as it is completely excluded from the porous packing causing K_{SEC} to approach 0 as the value of ΔS is substantially negative.

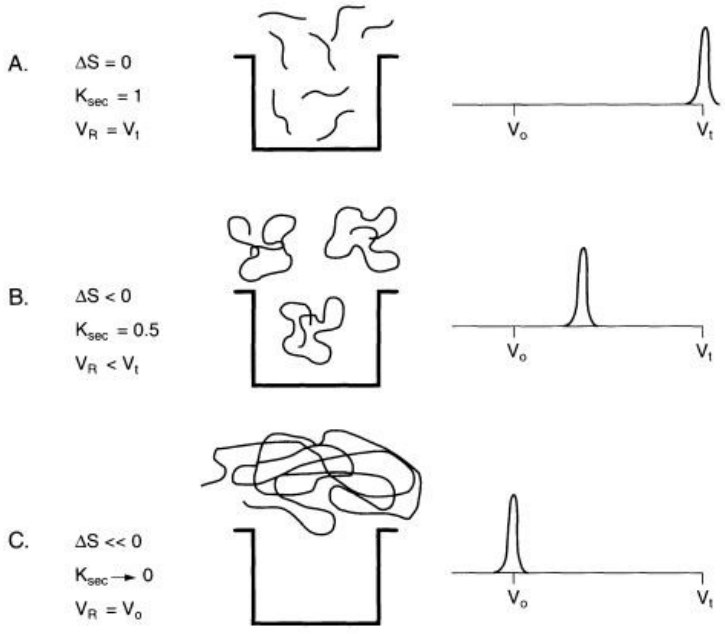

Figure 2.3: Schematic of the influence of molecule size on ΔS and K_{SEC}. Adapted from Mori and Barth [27].

It is important to note that in real SEC, distribution coefficients may not be exclusively determined by the entropy change. This is especially true with charged polymers, as it is often difficult to suppress enthalpic interactions completely [32].

2.6 The Universal Calibration Curve

Grubisic et al. [33] showed that SEC retention of different sets of polymers (including block and graft copolymers, PVC, PMMA, polybutadienes and poly(phenyl siloxanes)) yielded a common curve. An updated version of this curve is shown in Figure 2.4. Fundamentally, the calibration curve is a representation of the hydrodynamic volume as a function of elution volume, V_e, and describes how molecules of different sizes elute from the size-exclusion chromatography column.

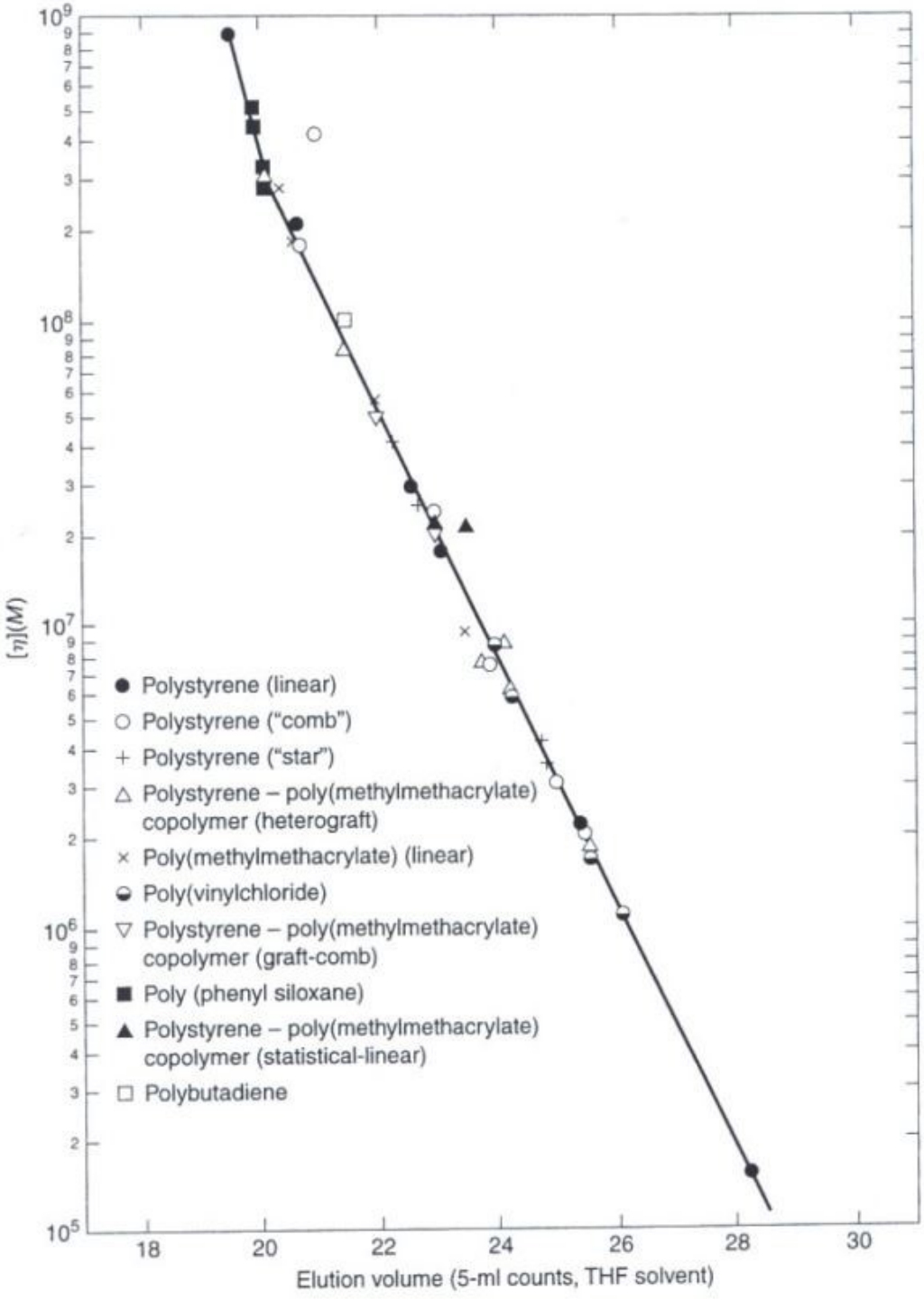

Figure 2.4: Universal calibration curve for size-exclusion chromatography. Reproduced from [33].

As represented in Figure 2.4, the hydrodynamic volume is the product of the polymer molecular weight, M, and intrinsic viscosity, $[\eta]$, and is proportional to the size of the polymer chains in solution given by [27]

$$[\eta]M = \phi\left(\overline{r_0^2}\right)^{3/2}\beta^2 \tag{2.7}$$

where the intrinsic viscosity is a measure of a solute's contribution to the viscosity of a solution [34], r_0^2 is the root-mean-square end-to-end distance of the polymer chain. Finally, β and ϕ are constants that depend on the type of solvent and polymer.

Another important expression that relates intrinsic viscosity to molecular weight is the Mark-Houwink equation [35]

$$[\eta] = KM^a \tag{2.8}$$

where a and K are coefficients for a given polymer dissolved in a specified solvent at a fixed temperature. The exponent a can be considered to be a conformational parameter of the macromolecule: the chain assumes a more spherical conformation when the value of a is close to 0 (no intrinsic viscosity dependency on molecular weight), and a more rigid-rod conformation as the value approaches 2 [27, 35]. The usual value for random-coil polymers varies from 0.5 in a poor solvent to 0.8 in a good solvent [4].

Considering that polymers with same hydrodynamic volume elute at the same time from the SEC columns, and in relation to the universal calibration presented in Figure 2.4, one may write

$$M_{std}[\eta]_{std} = M_x[\eta]_x \tag{2.9}$$

where the subscripts "*std*" and "*x*" indicate data of a calibration standard (i.e. polystyrene) or an unknown polymer, respectively. Combining Equations (2.8) and (2.9) and solving for M_x yields

$$\log M_x = \frac{1}{1+a_x}\log\frac{K_{std}}{K_x} + \frac{1+a_{std}}{1+a_x}\log M_{std} \tag{2.10}$$

Equation (2.10) allows the molecular weight of an unknown polymer sample to be calculated using the data from the calibrating polymers exiting the column at the same elution volume, as long as the values for K_x and a_x are available.

2.7 Essential Chromatography Concepts

2.7.1 Molecular Weight Distribution and Polydispersity

For polymers, molecular weight is a significant factor affecting properties such as tensile strength, melt viscosity, solubility, and considerably more [4,27]. These properties determine the polymer processing and end use applications. Most synthetic polymers are composed of many chains of different molecular weights that result in characteristic molecular weight distributions (MWD). As shown in Figure 2.5, each polymer will have a molecular weight distribution with a characteristic shape and breadth, depending on the polymerization mechanism and conditions [27]. This is important because different samples of the same polymer can have the same average chain length but very different chain length distributions [36]. Size-exclusion chromatography can be used to obtain molecular weight averages, which are the statistical moments of the molecular weight distribution, in addition to the full MWD. Figure 2.6 shows an example of the location of these moments within the MWD of a polymer. The three ratios of moments most commonly calculated are the number-average (M_n), weight-average (M_w), and z-average (M_z) molecular weights: M_n is more sensitive to molecules of low molecular weight, while M_w and M_z are more sensitive to molecules of high molecular weight [27, 36].

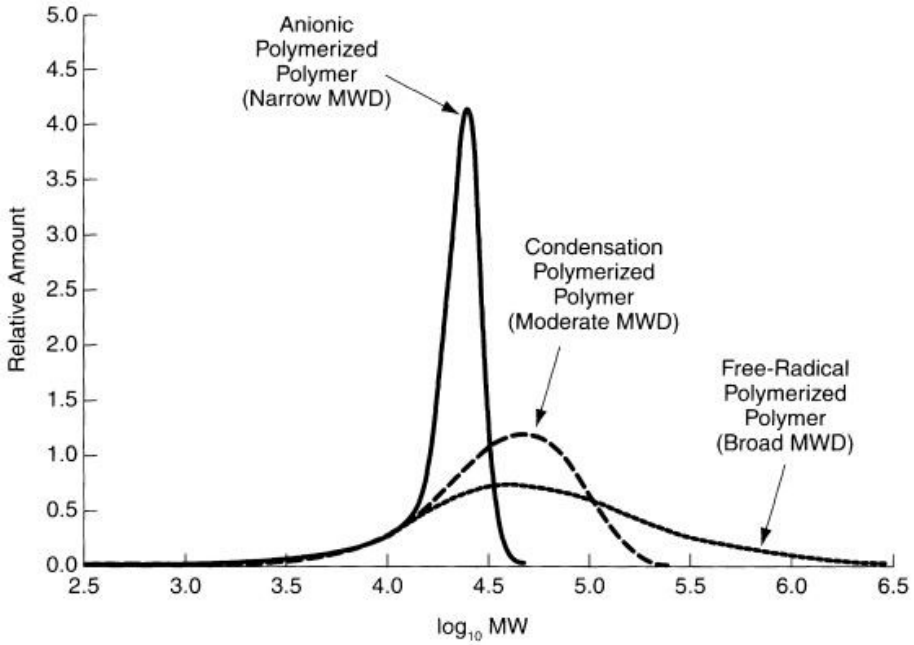

Figure 2.5: Molecular weight distributions of polymers made with different polymerization mechanisms [27].

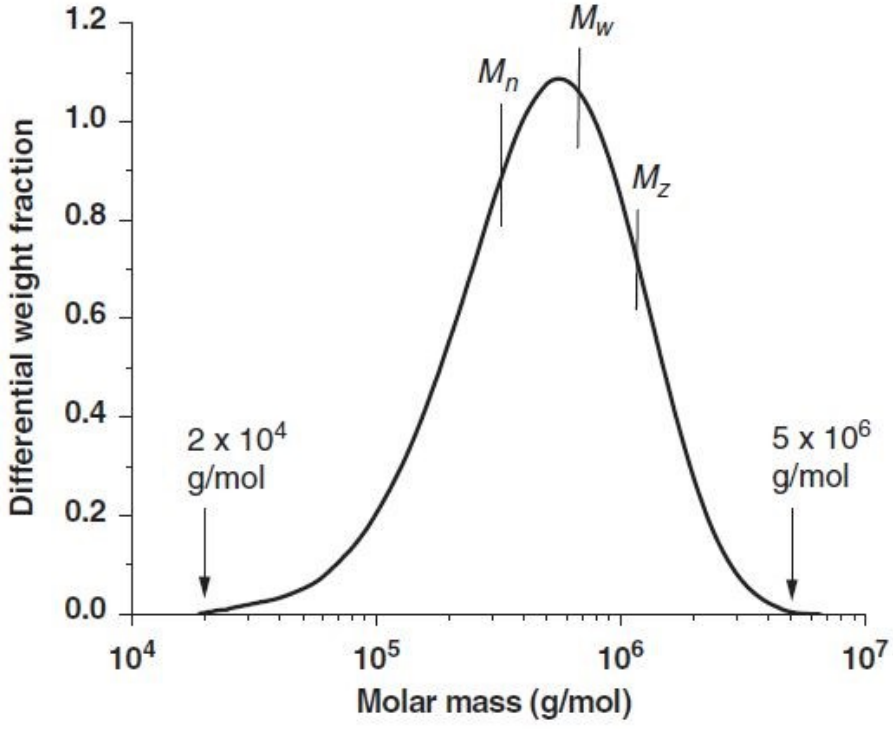

Figure 2.6: An example of MWD for a polymer and the location of M_n, M_w, M_z [8].

The width of the MWD is described as the polydispersity (PDI), and is calculated by taking the ratio of M_w/M_n [4, 8, 26]. PDI has a value equal to or greater than 1. As the polymer chains approach uniform chain length, PDI approaches unity and the polymer is considered to be monodispersed. Table 2.1 shows the significant utility of M_n, M_w, and PDI when describing the physical properties of synthetic polymers. For example, as the broadness of the MWD decreases, the tensile strength and toughness of the polymer increases. However, as the MWD becomes narrower, the polymer becomes more difficult to process. Therefore, SEC can provide vital information to predict the processability and material properties of a polymer.

Table 2.1: General correlations of M_w or MWD on some polymer properties [4].

	Tensile Strength	Yield Strength	Toughness	Brittleness	Melt Viscosity	Chemical Resistance	Solubility
Increase molecular weight	+	+	+	+	+	+	-
Narrow MWD	+	-	+	-	+	+	0

Key: +, property goes up; −, property goes down; 0, little change.

2.7.2 Retention and Selectivity

Figure 2.7 illustrates an example of concentration profiles as a function of time for the separation process in HPLC. In column chromatography, sample species travel through the column at different velocities and elute at different times. The molecules of a given species become more spread out as it migrates through the column, creating a volume called a band [8]. Each band that exits the column is described by a peak in the chromatogram. As a result, the identity of a given solute can be determined using the time from sample injection to the appearance of the peak in the chromatogram, or retention time (t_R), while the concentration of each solute is proportional to the area under the peak [4, 8, 37].

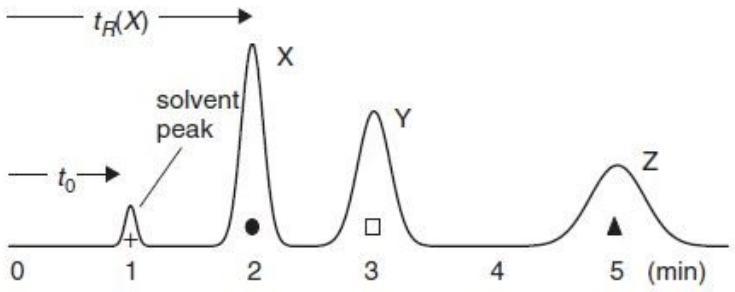

Figure 2.7: Example of a chromatogram with solute molecules X, Y, and Z. Adapted from [8].

The retention factor, *k*, is a measurement of the time that a component exists in the stationary phase relative to the time it exists in the mobile phase [38]. Snyder and Kirkland [8] defined the retention factor as

$$k = K\psi \tag{2.11}$$

where $K = C_s/C_m$ is the equilibrium constant between the mobile and solid phase, and $\psi = V_s/V_m$ is the phase ratio of stationary phase and mobile phase volumes. A solute exists in either the mobile or stationary phase, so that if *R* represents the fraction of molecules in the mobile phase, the fraction in the stationary phase must be *1- R*. Therefore Equation (2.11) can be written as

$$k = \frac{1 - R}{R} \tag{2.12}$$

The retention time, t_R, of a solute can be defined as the length of column, *L*, divided by the velocity of the solute u_s

$$t_R = \frac{L}{u_s} \tag{2.13a}$$

Likewise, the retention time of the solvent t_0, would be the length of the column divided by the average mobile phase velocity, u_0

$$t_0 = \frac{L}{u_0} \tag{2.13b}$$

Combining Equations (2.13a) and (2.13b) gives

$$t_R = \frac{t_0 u_0}{u_s} \tag{2.13c}$$

If it is assumed that, on average, u_s is equal to the fraction of molecules in the mobile phase times the velocity u_0 of the solvent, then

$$u_s = u_0 R \tag{2.14}$$

Therefore, combining Equations (2.12) and (2.13c) with Equation (2.14) gives

$$t_R = t_0(1 + k) \tag{2.15}$$

or

$$k = \frac{t_R - t_0}{t_0} \tag{2.16}$$

2.7.3 Peak Width and Efficiency

As shown in Figure 2.8, under ideal conditions it is assumed that a chromatogram will exhibit a symmetrical, Gaussian shape given by [39]

$$y = \frac{1}{\sqrt{2\pi\sigma^2}} e^{\frac{-(t-t_R)^2}{2\sigma^2}} \tag{2.17}$$

where σ is the standard deviation, σ^2 is the variance, and y is the concentration. It is important to note that actual peaks in a chromatogram will occasionally deviate from a symmetrical shape, exhibiting peak tailing. There can be several possible causes for tailings such as contamination, column overload, plugged voids, strength of solvent, or extra-column peak broadening [8].

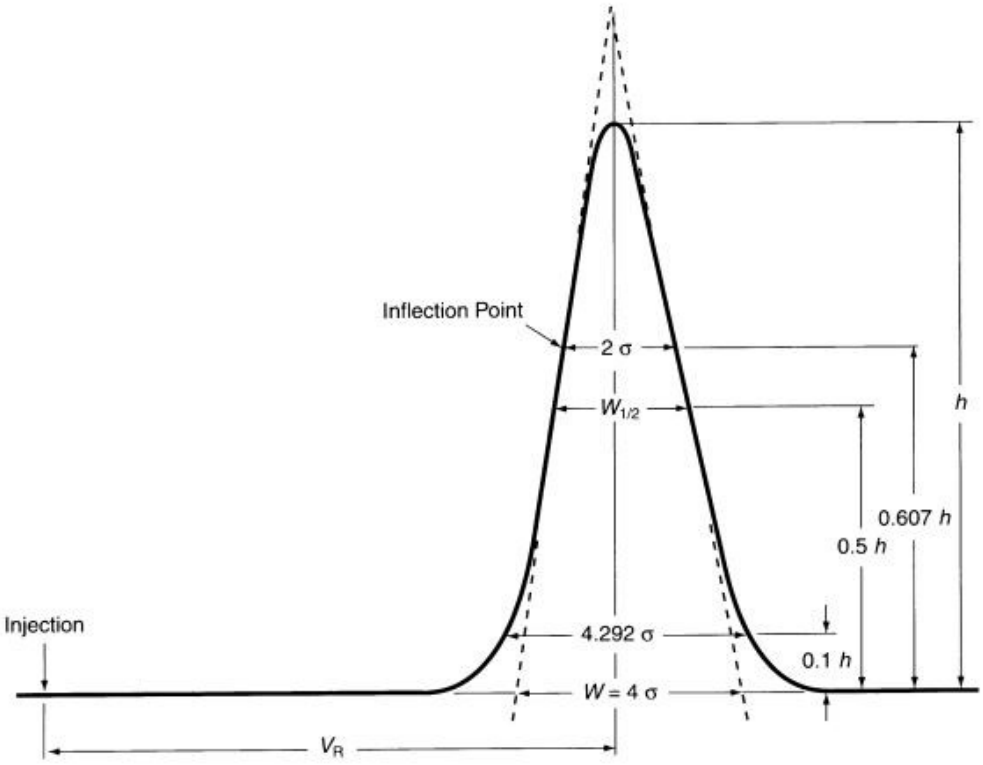

Figure 2.8: Ideal Gaussian-shaped chromatographic peak [23].

The efficiency of the column is a measure of mass transfer resistances. The most commonly cited parameter of column efficiency is expressed as the theoretical plate number, N [40]

$$N = 16\left(\frac{t_R}{W}\right)^2 \tag{2.18}$$

where W is the baseline peak width, as shown in Figure 2.8. However, peak width can be measured more precisely by determining the half-height peak width, $W_{1/2}$ (see Figure 2.8). Using this parameter, Equation (2.18) becomes

$$N = 5.54\left(\frac{t_R}{W_{1/2}}\right)^2 \tag{2.19}$$

Columns with high plate numbers are considered more efficient than columns with lower plate numbers. Explicitly, a column with a high number of theoretical plates will have a narrower peak at a given retention time than a column with a lower N number.

2.7.4 Band Broadening

As the band of the injected polymer sample travels through the column, the band will start to become more spread out, in the direction of flow, because of the difference in molecular sizes of the polymer [41]. The amount that the band broadens is directly related to the resolution of the column. The resolution of the chromatogram depends on the polydispersity of the polymer, pore volume, and slope of the calibration curve [27]. However, other factors also interfere with the separation process and negatively affect chromatographic resolution. An accurate understanding of the extra column effects is crucial to measuring band broadening. These effects are due to extra-column volumes from the sample injection, detector cell, and interconnecting tubing. Small scale columns packed with small particles are especially prone to extra column band broadening. In addition to extra-column effects, mass transfer resistances can have a significant effect on the band broadening process.

Several studies of SEC involving band broadening effects [41-44] and its correction [45-47] exist in the literature. The study of peak broadening involves the summation of independent factors treated as their second moments, or variances (σ^2), according to [41-47]

$$(\sigma_L^2)_{total} = (\sigma_L^2)_{inj} + (\sigma_L^2)_{detect} + (\sigma_L^2)_{tubing} + (\sigma_L^2)_{column} \tag{2.20a}$$

where the last term is a measure of band broadening that occurs within the column, expressed as

$$(\sigma_L^2)_{column} = \underbrace{(\sigma_L^2)_A}_{\text{axial diffusion}} + \underbrace{(\sigma_L^2)_E}_{\text{eddy diffusion}} + \underbrace{(\sigma_L^2)_{MP}}_{\text{mobile-phase mass transfer}} + \underbrace{(\sigma_L^2)_{SP}}_{\text{stationary-phase mass transfer}} \tag{2.20b}$$

2.8 Theories for Modeling Size Exclusion Chromatography

Several models of SEC column exist in the literature [48-53]. Ruthven [54] classified mathematical modeling of isothermal adsorption and chromatography into three general categories: equilibrium theory, plate theory, and rate models.

2.8.1 Equilibrium Theory

As previously discussed in Section 2.1.2, the equilibrium theory assumes an equilibrium between the mobile and stationary phase, while neglecting axial dispersion and mass transfer resistances. For chromatographic columns with fast mass transfer rates, the equilibrium theory is effective at predicting retention times of elution peaks, but fails to accurately illustrate peak broadening when mass transfer resistances are significant [55].

2.8.2 General Plate Theory

Martin and Synge [56] were the first to apply plate theory to liquid chromatography systems. In the plate model, the chromatographic column is divided into *N* number of sequential separation zones, as illustrated in Figure 2.9. The zones have a specific length, such that within them there is complete equilibration of the solute between the mobile and stationary phases [57]. The zones are referred to as *theoretical plates*, and their individual lengths in the column are called the *height equivalent to a theoretical plate* (HETP) or the *plate height*, *H* [56].

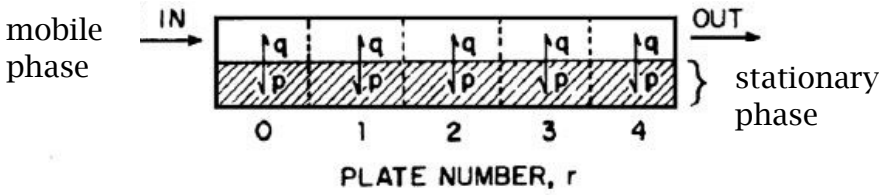

Figure 2.9: Representation of plate theory. Adapted from [4].

In Figure 2.9, q and p are the fraction of the total solute in the mobile and stationary phases respectively, with $q + p = 1$. The flow of the mobile phase is simulated by the sequential displacement of the top mobile phase section one plate to the right. We can designate the number of times this column displacement has taken place following the initial injection as n. As the volume is displaced, only a fraction of solute q in each plate is carried over the next plate, leaving a fraction of the solute behind, p. The solute re-establishes equilibrium in each new plate as the displacement process repeats. A binormal distribution function can be used to describe the solute distribution between many neighbouring plates by estimating the fraction of the original solute being in the r^{th} plate following n displacement is [58]

$$W(n,r) = \frac{n!}{r!\,(n-r)!} q^r p^{n-r} \tag{2.21}$$

Typically, chromatographic columns possess large plate numbers, which results in the binomial solute distribution becoming identical to the Gaussian distribution function [58]. With algebraic transformation, the plate model can predict a Gaussian elution profile. Expressed in terms of

concentration, retention volume V, peak retention volume V_r, sample weight W, and p, the fraction of solute in the stationary phase is [57]

$$c = \frac{W}{\sqrt{\frac{2\pi V_r^2}{N}}} e^{\frac{-N(V-V_r)^2}{2pV_r^2}} \tag{2.22}$$

Comparing Equation (2.22) with the general Gaussian function (Equation 2.17), one can derive the relationship

$$N = \frac{pV_r^2}{\sigma^2} \tag{2.23}$$

Other results of the general plate theory are [7,10]

$$H = \frac{L}{N} \tag{2.24}$$

and

$$H = \sum_i H_i \tag{2.25}$$

where L is the length of the column and H_i is the individual plate height contribution of independent column dispersion effects. In summary, for size-exclusion chromatography, the general plate theory predicts that the peak shape is Gaussian, and N is directly proportional to column length.

However, as useful and as simple this model is for studying chromatographic elution profiles, it does have limitations. For multicomponent liquid chromatography, equilibrium stages may not be assumed to be equal for different solutes, thus restricting plate models to single-component liquid chromatography modeling [59].

2.8.3 Rate Models

Rate models refer to models containing a rate expression to describe the interfacial mass transfer effects between the mobile and stationary phase. Typically, mathematical models of chromatography contain two sets of derived differential mass balance equations: one for the bulk-fluid phase and the other for the solid phase for each compound. These models also include initial and boundary conditions and the equilibrium isotherms of the relevant compounds.

Glueckauf and Coates [60] proposed a solid film resistance which assumed a linear driving force between the equilibrium concentrations in the stationary phase and the average concentrations in the stationary phase. This model was used due to its simplicity, but it could not describe mass transfer restrictions in the particle phase. A fluid film mass transfer mechanism [54] interprets the linear driving force differently. The concentration difference of the solute between the surface of a particle and that in the surrounding mobile phase is defined as the driving force. It is assumed that there is an external, stagnant fluid film between the particle surface and the bulk fluid phase the exerts a mass transfer resistance. If the concentration gradient inside the solid phase is ignored, then this model becomes a lumped particle model [61].

Chapter 3 Materials and Methodology

3.1 Introduction

Before any simulations are carried out, it is important to detail instrument specifications and polymer properties. This will allow us to have a thorough understanding of the system being modeled in the simulations.

3.1.1 Instrumentation

Size-exclusion chromatography (Polymer Char, Valencia, Spain) was used to measure MWD using three linear columns (PLgel Olexis, 13 μm gel particles, and 300 mm × 7.5 mm) at 145 ºC. Narrow-MWD polystyrene standards were used to calibrate the columns. The linear molecular weight operating range of the columns varies from 2,000 to 10,000,000 g/mol. A 200 μL volume of polymer solution was injected into the columns at a flow rate of 1.0 mL/min of trichlorobenzene (TCB). The GPC was equipped with an infrared detector, used as a mass detector. The MWDs of all samples were determined using the universal calibration curve and Polymer Char software package following standard procedures.

3.1.2 Polymers

The validity of a model can be judged by its ability to predict actual experimental results. Since they possess a narrow distribution and monodispersed composition, polystyrene standards with various average molecular weights, supplied by Polymer Laboratories, were used to compare experimental results to model predictions. The properties of the polystyrene standards are listed in Table 3.1.

Table 3.1: Properties of polystyrene standards as provided by Polymer Laboratories.

M_p	M_n	M_w	PDI
1 310	1 220	1 300	1.07
5 000	4 840	4 970	1.03
30 300	29 800	30 150	1.02
50 400	48 200	49 300	1.03
96 000	92 350	94 650	1.03
135 000	131 200	133 750	1.02
186 000	177 864	182 900	1.03
325 000	314 400	321 200	1.03
1 124 000	1 043 700	1 103 650	1.06
1 460 000	1 400 000	1 444 000	1.04
2 320 000	2 221 000	2 316 000	1.04
3 900 000	3 634 000	3 794 000	1.05

3.2 Multicomponent Rate Model for Size Exclusion Chromatography

3.2.1 Model Assumptions

For the modeling of size-exclusion chromatography, the column was divided into the bulk-fluid phase and the particle phase. Figure 3.1 shows a schematic of a fixed-bed axial flow size-exclusion chromatography column. The model was formulated under the following assumptions:

1. The column is isothermal
2. Different solutes do not interact with each other
3. The stagnant fluid and macropore surface inside the particles reach instantaneous equilibrium.
4. Diffusional and mass transfer coefficients are constant
5. Solid particles inside the column are spherical and have uniform in diameters
6. The packing density is constant along the column
7. No convective flow inside the macropores
8. Concentration gradients in the radial direction are negligible

The solution of the multicomponent rate model requires complex and time-consuming numerical techniques. Moreover, the physical and thermodynamic phenomena are not completely understood. Both these factors necessitate these basic assumptions in order to handle the problem more efficiently, while remaining realistic.

It is important to note that column packing is usually not spherical with a uniform diameter. In these cases, an "effective" particle diameter may be used [10]. Moreover, if the process is not isothermal, physical and isotherm parameters would be time or zone dependent. Mass transfer between the bulk-fluid phase and the stationary phase is characterized by the fluid film mass transfer mechanism.

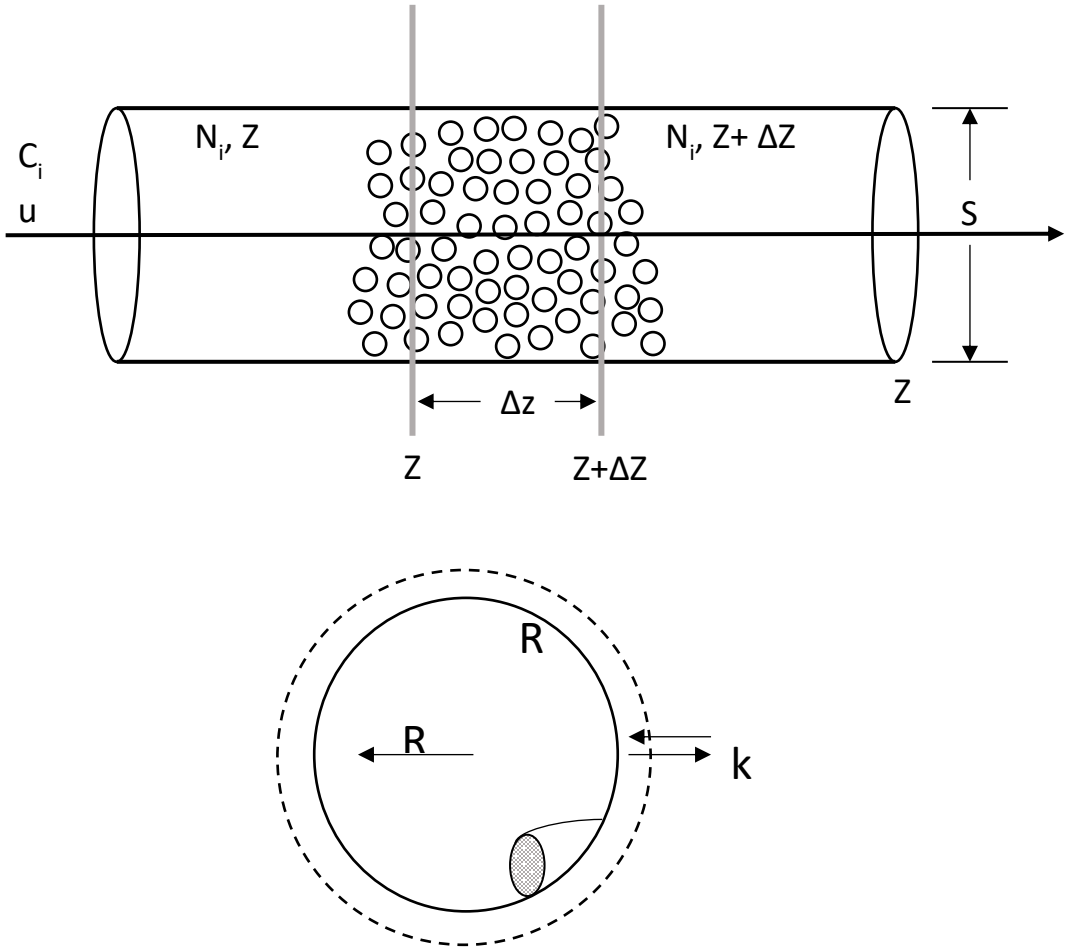

Figure 3.1: Schematic for bulk-fluid phase and porous particle phase.

3.2.2 Differential Mass Balance of Bulk-Fluid Phase

All properties at any given cross section in the column illustrated by Figure 3.1 are constant and so are the concentrations of the separate components. We shall consider the concentration $C_{m,i} = C_i$ (mobile phase) and $C_{s,i}$ (stationary phase) as a function of time, t, and column length, z.

If V is the volume of the mobile phase travelling through the column, the integral mass balance states that the area of the elution profile in the coordinate system (C_i, t) at the outlet of the column of length z is equal to the area of the injected profile if $C_{s,i} = 0$. While the *sum* of the areas in the mobile ($C_{m,i}$, z) and stationary ($C_{s,i}$, z) phases is constant, the area of the profile in the coordinate system (C_i, z) is not because the equilibrium isotherm is usually not linear. Therefore, the determination of these profiles requires the examination of the differential mass balance.

From Figure 3.1, the difference between the amount of the component i that enters a slice of thickness Δz during time Δt and the amount that leaves the slice in the same time is equal the amount accumulated in the slice. The flux of component i that enters the slice, $N_{i,z}$, is [2]

$$N_{i,z} = \varepsilon S \left(u C_i - D_{L,i} \frac{\partial C_i}{\partial z} \right) \Big|_{z,t} \tag{3.1a}$$

where ε is the total porosity of the column packing, $S = \pi d^2/4$ is the cross-sectional area of the column, u is the average bulk-fluid phase velocity, C_i is the local solute concentration in the bulk-fluid phase, $D_{L,i}$, is the axial dispersion coefficient of the compound in the bulk-fluid phase, and z is the length along the column. The first term within the brackets of Equation (3.1a) is related to convection, while the second term accounts for the axial dispersion of the elution profile due to molecular and eddy diffusion.

It follows that the flux of the component that exits the slice is

$$N_{i,z}\big|_{z+\Delta z} = \varepsilon S \left(u C_i - D_{L,i} \frac{\partial C_i}{\partial z} \right) \Big|_{z+\Delta z,t} \tag{3.1b}$$

The rate of accumulation in the slice of volume $S\Delta z$ is [2]

$$S\Delta z\left(\varepsilon\frac{C_i}{\partial t}+(1-\varepsilon)D_{L,i}\frac{\partial C_{s,i}}{\partial t}\right)\Big|_{\bar{z},t} \tag{3.1c}$$

Assuming that u and $D_{L,i}$ are constant along the column, and allowing Δz to approach 0, the following differential mass balance for a component i in the bulk-fluid phase can be derived

$$\frac{\partial C_i}{\partial t}+F\frac{\partial C_{s,i}}{\partial t}+u\frac{\partial C_i}{\partial z}=D_{L,i}\frac{\partial^2 C_i}{\partial z^2} \tag{3.2}$$

where F is the ratio of the volumes of the stationary and mobile phase, V_s/V_m, which is equal to (1-ε)/ε.

3.2.3 The Equilibrium-Dispersive Model

The relationship between the local concentrations of the solute in the mobile and stationary phases is given by a kinetic equation that relates $\partial C_{s,i}/\partial t$ to both phase compositions. If the mass transfer kinetics across the bulk-fluid and stationary phases are very fast, then the phases are close to equilibrium [2]. Hence, it can be stated

$$C_{s,i}=q_i=f_i(C_1,C_2,\dots,C_i,\dots,C_n) \tag{3.3}$$

where $C_{s,i}$ is the instantaneous concentration of the component i in the stationary phase and q_i is the stationary phase concentration of the component when in equilibrium with the concentrations in the mobile phase. f_i is the adsorption isotherm used to represent the different functional relationships.

It has been shown by Giddings [62] and van Deemter et al. [63] that when mass transfer kinetics are fast, Equations (3.2) and (3.3) can be replaced by the following expression

$$\frac{\partial C_i}{\partial t} + F\frac{\partial q_i}{\partial t} + u\frac{\partial C_i}{\partial z} = D_{L,i}\frac{\partial^2 C_i}{\partial z^2} \tag{3.4}$$

where $D_{L,i}$ is the axial dispersion coefficient given by

$$D_{L,i} = \frac{HL}{2t_0} = \frac{Hu}{2} \tag{3.5}$$

where H is the plate height for the component being studied, and t_0 is the retention time of the solvent. Equation (3.4) is called the equilibrium-dispersive model and assumes that all contributions to band-broadening are lumped into an axial dispersion term.

3.2.4 The General Rate Model

The general rate model attempts to describe all possible contributions to the mass transfer kinetics simultaneously. It takes into account the axial dispersion (molecular diffusion and eddy diffusion), the external film mass transfer resistance, the sum of the contributions of pore and surface diffusion, and the rate of adsorption-desorption. The general rate model consists of two differential mass balance equations for the solute: one for the mobile phase and the other for the stagnant liquid phase inside the particle. The mass balance equation is given by

$$\frac{\partial C}{\partial t} + F\frac{\partial \bar{q}}{\partial t} + u\frac{\partial C}{\partial z} = D_L\frac{\partial^2 C}{\partial z^2} \tag{3.6}$$

where $\bar{q}$ is the average stationary phase concentration over the entire particle.

The rate of adsorption averaged over the spherical particle is

$$\frac{\partial \bar{q}}{\partial t} = \frac{3}{R_p M_F} \tag{3.7}$$

where M_F is the mass flux of the solute from the mobile phase to the particle surface.

Combining Equations (3.6) and (3.7) the mass balance for a single component in the mobile phase can be derived as

$$-D_L \frac{\partial^2 C}{\partial z^2} + u\frac{\partial C}{\partial z} + \frac{\partial C}{\partial t} + \frac{3k_f(1-\varepsilon)}{R_p \varepsilon}\left(C - C_p\big|_{r=R_p}\right) = 0 \tag{3.8}$$

and the differential mass balance of the solute in the stagnant liquid phase is given by

$$\varepsilon_p \frac{\partial C_p}{\partial t} + (1-\varepsilon_p)\frac{\partial C_s}{\partial t} = D_p\left(\frac{\partial^2 C_p}{\partial r^2} + \frac{2}{r}\frac{\partial C_p}{\partial r}\right) \tag{3.9}$$

where ε_p is the porosity of the particle, C_p is the concentration of the solute inside the pores, C_s is the concentration of the solute adsorbed, and D_p is the diffusion coefficient of the solute in the pores. Together, Equations (3.8) and (3.9) are known as the general rate model of chromatography.

3.2.5 Lumped Kinetic Model

Morbidelli et al. [64] argued that the solution of the general rate model is complicated and requires sophisticated numerical algorithms, which means longer computation times. The study of the lumped kinetic models [65-67] shows that, as long as equilibrium kinetics are relatively quick, and the column efficiency exceeds 50 theoretical plates, the elution profile resembles a Gaussian distribution.

The lumped kinetic model combines the mass balance equation, Equation (3.2), with a kinetic equation. It describes how the rate of variation of the concentration of each component in the stationary phase is related to their respective concentrations in both phases and to the equilibrium concentration in the stationary phase [60]. While kinetic models are considered to be more accurate than the equilibrium-dispersive model, Equation (3.4), there is a negligible difference between them when the column efficiency exceeds a few hundred theoretical plates [2].

One of the most popular forms of the lumped kinetic model is referred to as the *solid film linear driving force model,* and is given by [54]

$$\frac{\partial C_{s,i}}{\partial t} = k_m\left(q_i - C_{s,i}\right) \tag{3.10a}$$

where q_i is the equilibrium value of $C_{s,i}$ for a bulk-fluid phase concentration equal to C_i, and k_m is the lumped mass transfer coefficient. For each component in a system, Equation (3.10a) can be expressed as

$$\frac{\partial q_i}{\partial t} = k_{m,i}(q_i^* - q_i) \tag{3.10b}$$

where $k_{m,i}$ is the lumped mass transfer coefficient of component i and q_i^* is the stationary phase concentration at equilibrium related to the mobile phase concentrations through the competitive equilibrium isotherm, $q_i^* = f\ (C_j)$.

Since most chromatography processes have fast adsorption-desorption kinetics, instantaneous equilibrium between the stationary and mobile phase can be assumed. Ignoring the competition between the sample and the active components in the bulk-fluid phase, the adsorption equilibrium can be described by the Langmuir isotherm [68]

$$q_i^* = \frac{HC_p}{1 + K_{eq}C_p} \tag{3.10c}$$

where $H=K_{eq}q^{\infty}$ is the Henry constant and is equal to the slope of the linear isotherm, K_{eq} is the equilibrium constant, and q^{∞} is the loading capacity.

3.2.6 Initial and Boundary Conditions

The Initial Conditions

The initial conditions describe the state of the column at the beginning of the experiment, $t = 0$. Typically, in elution chromatography, the column is filled with a mobile phase that does not factor into the mass balances [69]. Therefore, the initial condition for the mobile phase is

$$C_i(z, t = 0) = 0 \quad \text{for } 0 \leq z \leq L \tag{3.11}$$

where L is the column length.

The Danckwerts Boundary Conditions

Carrying out a material balance over a small region at the entry point of the column, while considering diffusion and convection, yields the following result presented by Danckwerts [70]

$$\left[vC - D\frac{\partial C}{\partial z}\right]\Big|_{z=0} = vC_f \tag{3.12}$$

$$\left[\frac{\partial C}{\partial z}\right]\Big|_{z=L} = 0 \tag{3.13}$$

Equation (3.12) describes how the mass flux at the column inlet where the injection is made is equal to the mass flux achieved in a pipe having the same diameter as the column.

3.4 Input Variables, Discretization, and Solution to the ODE system

Multicomponent rate models consisting of one or more partial differential equations (PDE) can be solved using a variety of numerical methods [71-73]. The finite difference method is an easy numerical technique that can be used to discretize the mobile and particle phase equations [74]. However, a large number of discretization points are required to achieve an accurate, stable solution, resulting in larger computation times.

Figure 3.2 shows the numerical solution strategy for the simulation of the rate model. In this study, the finite element method was used because it is more efficient and accurate than the finite difference method. Using this discretization scheme, the partial differential equation is written as an ordinary differential equation (ODE). The resulting system of equations is solved using Matlab® 9.3.0. (The MathWorks, Inc., MA, USA) on a personal computer using the parameters listed in Table 3.2.

Table 3.2: Simulation parameters for the rate model.

Parameter	Source
length of column, L	measured
diameter of column, d	measured
volumetric flow rate, Q	measured
bed voidage, ε_b	correlation
accessible porosity, ε_p	fitted
axial dispersion coefficient, D_L	correlation
mass transfer coefficient, k_m	fitted
injection time, t_{inj}	measured
injection concentration, C_{inj}	measured
number of discretization points, nz	fitted

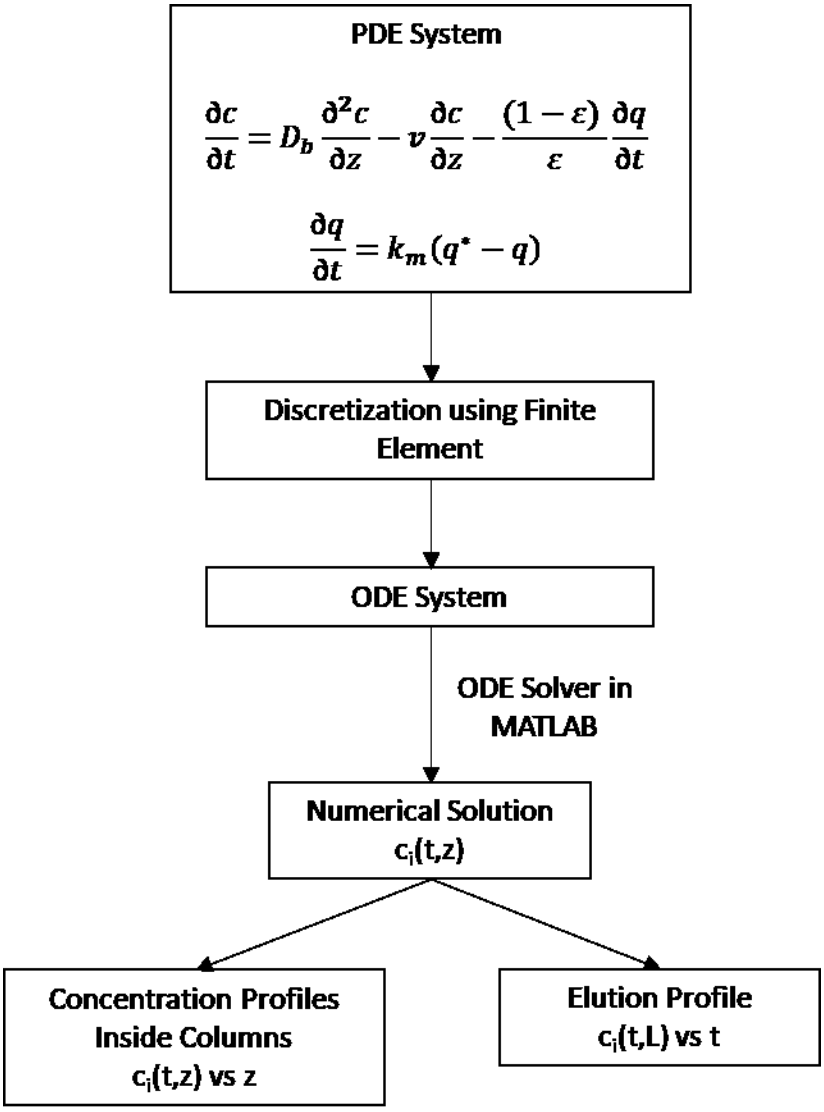

Figure 3.2: Numerical solution strategy

Chapter 4 Results and Discussion

4.1 Gaussian Distribution Predictive Model

Before the rate model was developed, a predictive model was used by generating a molecular weight distribution for each polystyrene standard, as shown in Figure 4.1. Knowing the PDI and molecular weight, one can successfully generate the molecular weight distribution (MWD) using a Poisson distribution as shown in Panel A. Panels B and C depict how the MWD is then split into multiple fractions by setting a molecular weight interval, d*MW*, and the concentration of polymer in each of the fractions is calculated as a percentage of the total area. Trends obtained from experimental data are used to calculate the first and second moments, μ and σ respectively, of each molecular weight fraction. The moments are then used to generate a normal distribution for each fraction. The final peak is obtained by adding all distributions, where the total concentration should be equal to the original injection concentration illustrated in Panel D.

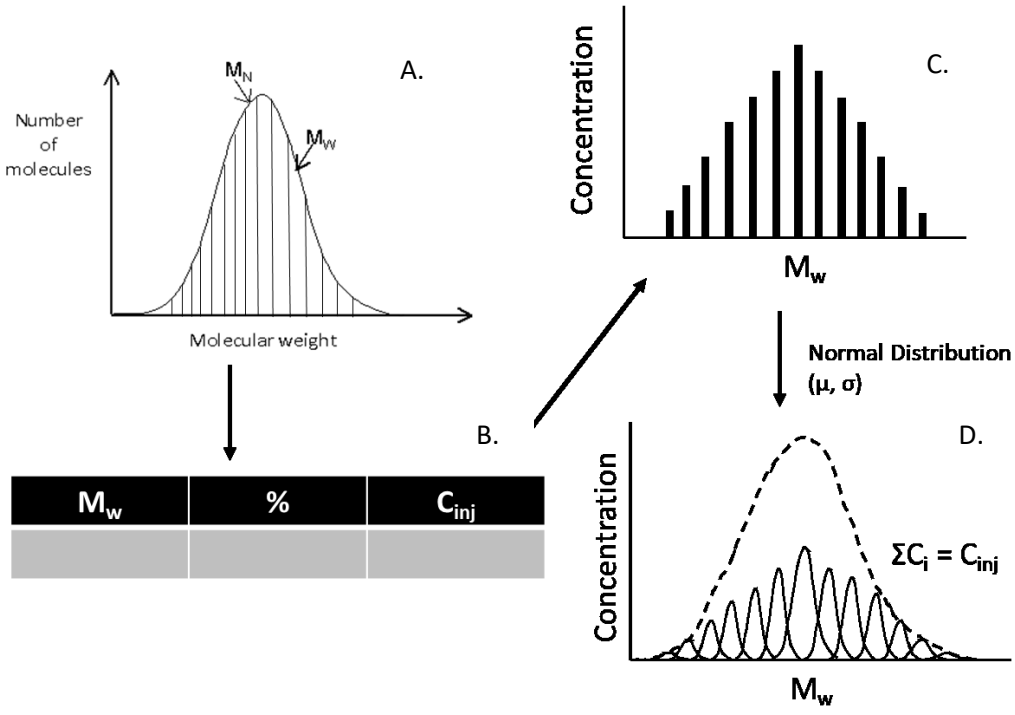

Figure 4.1: Illustration of the method for the Gaussian predictive model.

4.2 Determining Kinetic Rate Model Parameters

Table 4.1 shows the measured column parameter values that were held constant in each experiment and simulation. The injection concentration was also measured but varied for each run. Tracer injections of n-hexane were performed to determine the total column porosity, ε_t, using the following relationship [74]

$$t_0 = \frac{\pi d^2 L \varepsilon_t}{4Q} \tag{4.1}$$

where t_0 is the retention time of very small molecules such as n-hexane which totally permeates the macropores. Tracer injections eluted consistently at 26.6 minutes, and as a result, $\varepsilon_t = 0.67$.

de Klerk [75] investigated the variation of bed voidage in relation with column to particle diameter ratio where for large ratios it was found that $\varepsilon_b \approx 0.359$-$0.363$. The bed voidage of the column, ε_b, was assumed according to its large column to particle diameter ratio (>20).

Table 4.1: Parameter values used for simulation

Parameter	Value
length of column, L	90 cm
diameter of column, d	0.75 cm
volumetric flow rate, Q	1 cm^3/min
injection time, t_{inj}	1 s
bed voidage, ε_b	0.362

The axial dispersion coefficient, D_L, was determined from the column efficiency evaluated for each sample

$$\frac{L}{N} = \frac{2D_L \varepsilon_b}{u} \tag{4.2}$$

where u is the superficial velocity and N is the plate number.

The lumped mass transfer coefficient, k_m, was determined using a peak fitting method for several polystyrene standards. It was concluded that k_m between 0.1 - 1 s^{-1} was able to best fit the experimental data.

For the linear isotherm, the parameter H for each sample was determined from the first moment, μ, of the chromatographic curve, i.e., the elution time at the maximum peak height in relation to

$$\mu_x = \frac{L}{u}(\varepsilon_t + (1 - \varepsilon_t)H) \tag{4.3}$$

4.3 Parametric Study for Polystyrene Standards

Examining the sensitivities of parameters in the rate model is beneficial, since the findings can indicate which parameters effect the system more significantly. Thus, we can determine which parameters require a more rigid estimation and which parameters can be more broadly approximated.

4.3.1 Effect of the Axial Dispersion

The influence of D_L on the chromatogram is shown in Figure 4.2. The parameters used to obtain Figure 4.1 are detailed in Table 4.2. In addition, ε_p = 0.22, C_{inj} = 1.5 mg/mL, and the number of discretization points, nz = 200 were used. It can be seen from Figure 4.1 that as the axial dispersion becomes smaller, the simulated peak becomes narrower. It can be inferred from Equation (4.2), as D_L decreases, the plate number increases resulting in a narrower peak. Furthermore, when D_L < 1.2×10^{-4} cm^2/s, its influence on peak width becomes relatively inconsequential. As a result, we can conclude that the axial dispersion does not require a rigid estimation. In this work, it has been determined that the typical range for the axial dispersion coefficient is between D_L = $1.0\text{x}10^{-4}$ – $1.0\text{x}10^{-6}$ cm^2/s. It is important to note that the velocity of the solvent and particle size remains constant throughout the entirety of this work. If the velocity of the solvent or the particle size of the solid phase were increased, the value of the axial dispersion coefficient would also increase.

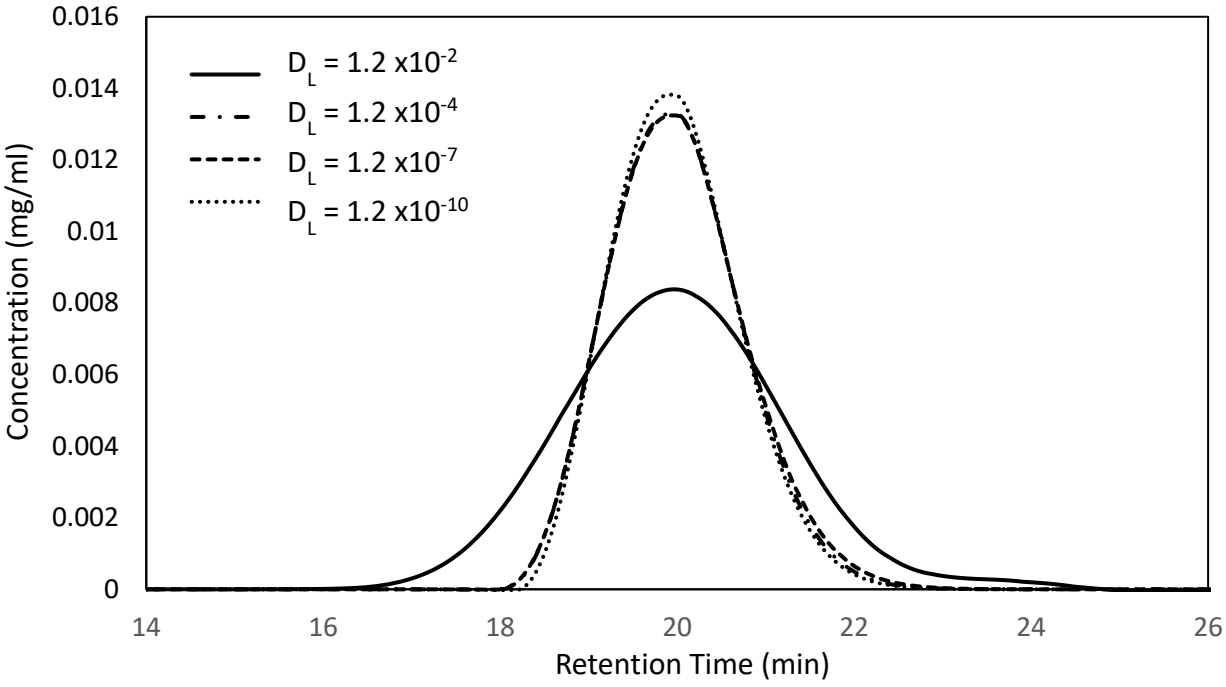

Figure 4.2 The effect of axial dispersion (cm^2/s) on elution profiles.

4.3.2 Effect of the Lumped Mass Transfer Coefficient

The effect of the lumped mass transfer coefficient on the chromatograms is illustrated in Figure 4.3. Consistent with Figure 4.2, ε_p = 0.22, C_{inj} = 1.5 mg/mL, and nz = 200 were used in the simulation. Figure 4.3 shows that the peak shape is significantly affected by the value of k_m. As k_m increases, the peak becomes sharper. A large discrepancy between each case is observed since the lumped mass transfer coefficient is related to the film and pore mass transfer resistances and has a significant impact on the solid linear driving force, as described by Equation (3.10a), which causes the peaks to become narrower as k_m increases.

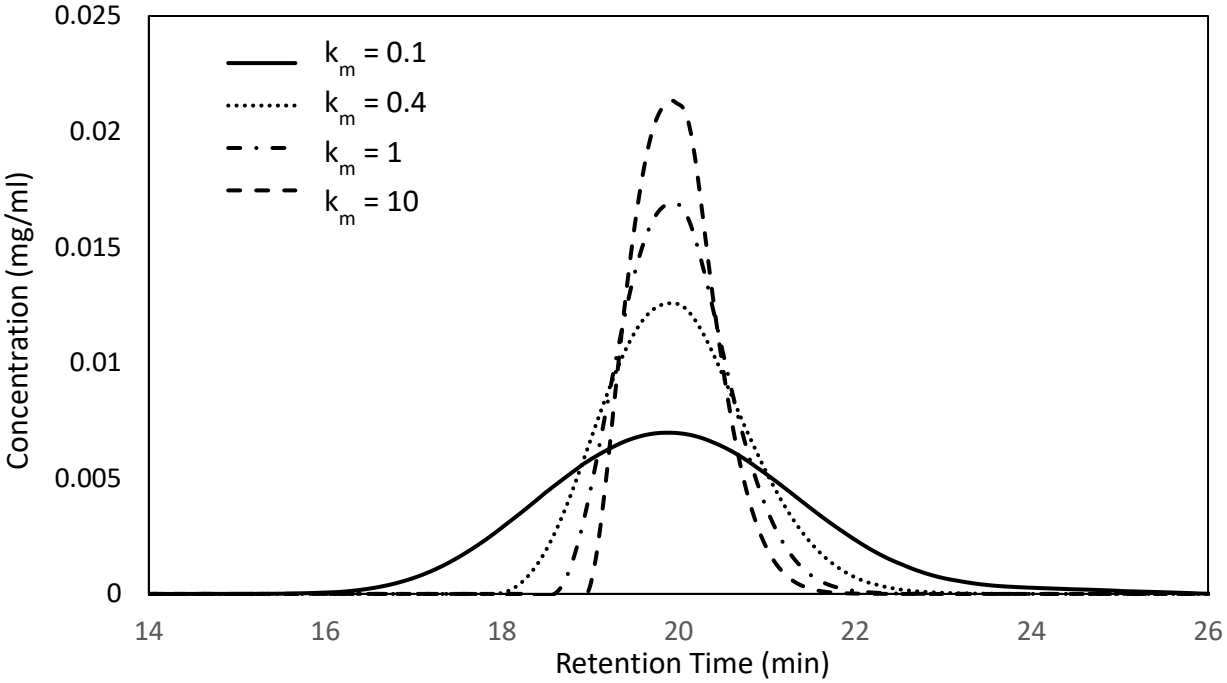

Figure 4.3 The effect of the lumped mass transfer coefficient (s^{-1}) on elution profiles.

Table 4.2: Parameter values used to study the effects of D_L, k_m, and nz

Figure	D_L (cm^2/s)	k_m (s^{-1})	nz
4.1	$1.20x10^{-2}$ $1.20x10^{-4}$ $1.20x10^{-7}$ $1.20x10^{-10}$	0.4	200
4.2	$1.20x10^{-4}$	0.1 0.4 1 10	200
4.3	$1.20x10^{-4}$	0.4	100 200 300 400

4.3.3 Effect of the Number of Discretization Points

The effect of discretization points on elution peaks is shown in Figure 4.4. As the number of discretization points, *nz*, increases, the simulated peak becomes sharper. This is expected since the amount of numerical dispersion in the simulation is directly proportional to *nz*. Increasing the number of points will increase resolution, it will also be more time consuming. Table 4.3 lists the simulation times ranging from 5 seconds to 5 minutes. Accepting 5 minutes is a relatively short amount of time to wait for an increase in peak resolution, all following simulations in this work use $nz = 400$.

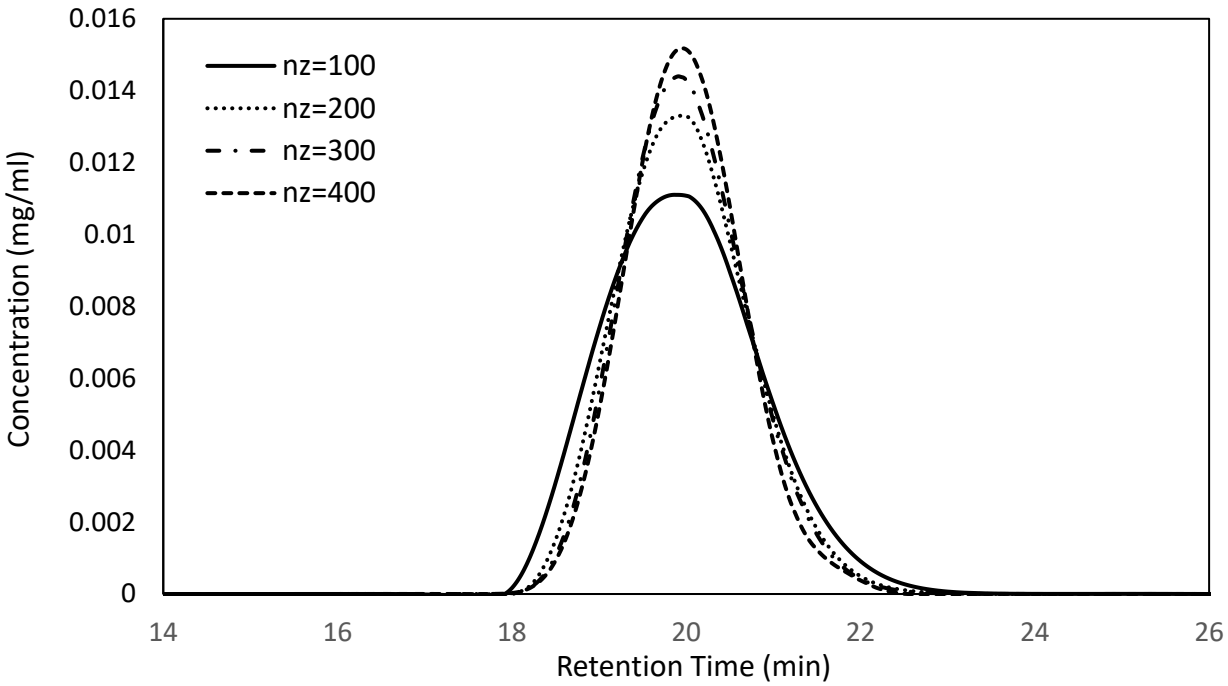

Figure 4.4 The effect of number of discretization points on elution profiles.

Table 4.3: Computation times for different number of discretization points.

Number of Discretization points, *nz*	Computation time (s)
100	5
200	33
300	107
400	235

4.4 Molecular Weight Trends

4.4.1 Accessible Porosity

Figure 4.5 shows how the accessible porosity of a solute depends on its hydrodynamic volume for several polystyrene samples. The elution times for each polystyrene standard was obtained from multiple historical data sources. The accessible porosity values were calculated from the corresponding elution times of each polymer using Equation (4.3). As expected, as the size of the molecule decreases, the more readily the molecules penetrate the pores. This is the crucial separation mechanism that defines size-exclusion chromatography. As a result, the accessible porosity is an important parameter when simulating SEC elution profiles. Using the same data presented in Figure 4.5, we can determine the accessible porosity of any polystyrene standard if the average molecular weight is known by plotting ε_p as a function of MW. The resulting fitted equation is:

$$\varepsilon_p = -0.039ln(MW) + 0.6465 \tag{4.4}$$

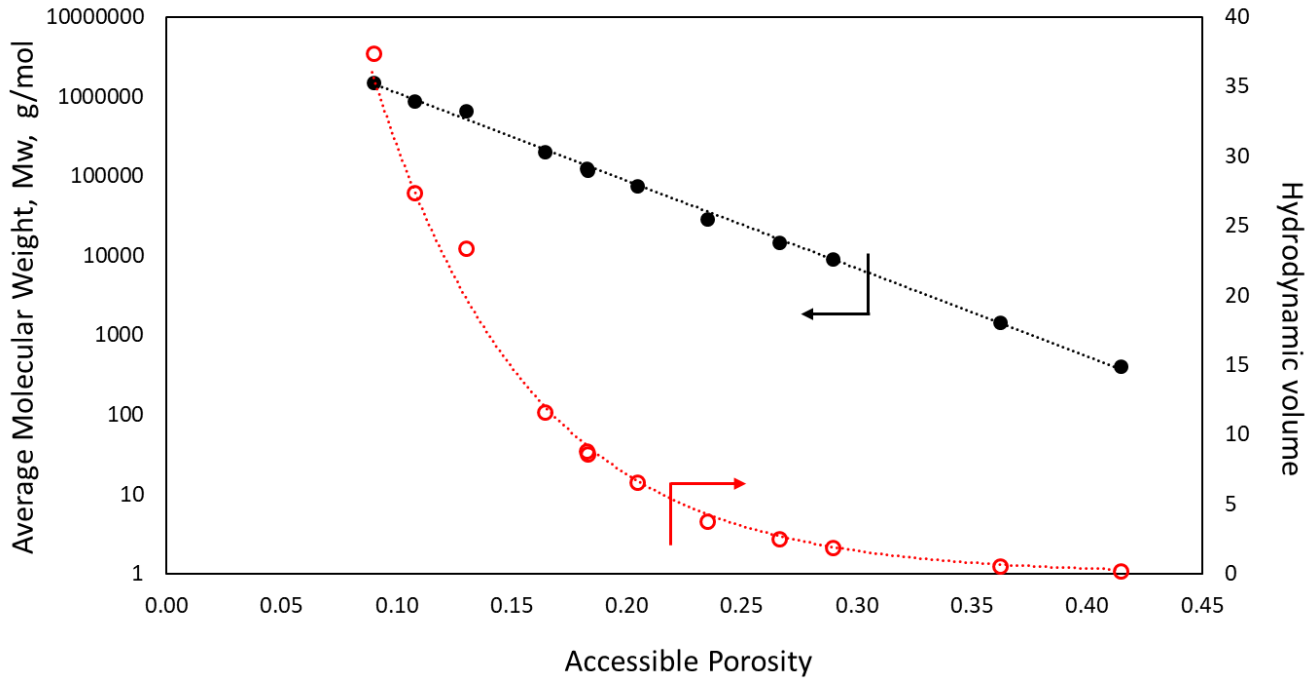

Figure 4.5: Accessible porosity as a function of size for various polystyrene samples. The red and black dots were experimentally collected. The corresponding dotted lines are trends.

4.4.2 Plate Number

Figure 4.6 shows how the number of plates is related to the molecular weight of polystyrene samples. The number of plates were calculated from historical and present data using Equation (2.19), where $W_{1/2}$ was measured manually from the corresponding elution profiles. From Section 2.7.3, the plate number is a measure of column efficiency, and is inversely proportional to the width of the peak. According to Figure 4.6, standards with lower molecular weights will experience a much larger plate number than those with higher molecular weights. This is because the plate number, N, is directly proportional to retention time and inversely proportional to peak width, as described by Equation (2.19). As a result, polystyrene standards with lower molecular weight averages and narrower MWDs will have larger N values compared to standards with higher averages and broader distributions.

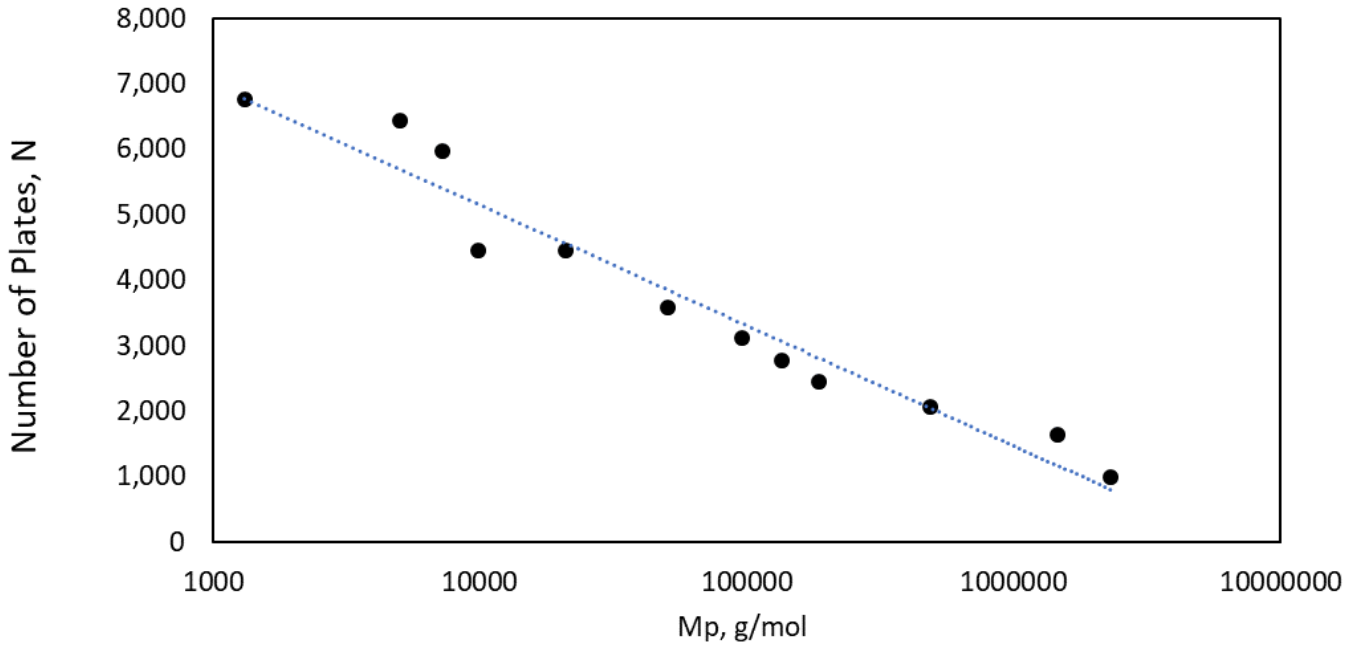

Figure 4.6: Plate number as a function of peak molecular weight. The black dots are experimentally obtained values. The blue dotted line shows the trend as the size of the polystyrene standard increases.

4.4.3. First and Second Moments

A Gaussian distribution, as described in Section 2.7.3, relies on two important moments to describe the shape of a set of points. The first moment is called the mean, μ, and is represented by the elution time at the peak of the elution profile. The second moment is called the variance, σ^2, and describes the peak width of the elution profile.

Figure 4.7 shows how the experimental elution times and peak widths (variance) vary with increasing peak molecular weight of polystyrene. As the average molecular weights of the polystyrene standard increases, they eluted faster from the column. As previously stated, this is because smaller molecules are able to enter the pores of the solid phase, are trapped and removed from the flow of the mobile phase (elute later), while molecules that are larger than the accessible porosity of the packing are excluded and thus suffer no retention (elute earlier). However, we observe an opposite trend in Figure 4.7b): the variance increases for larger polystyrene standards. This is likely caused by the polydispersities of the polystyrene standards, as samples with lower M_p also have lower PDI. Equation (2.10b) can also be used to consider other contributions to band broadening. The volume of the polystyrene samples in solution will contribute to the eddy diffusion term, while the axial diffusion term is dependent on the size of the polystyrene standard.

Figure 4.7 shows each sample of polystyrene possess its own first and second moment. Therefore, one can generate Gaussian distributions, using Equation (2.17), to describe the elution profile of each polystyrene standard if its mean and variance are known. From experimental results, we can find the relation between both moments and molecular weight, as described by the equations presented in Figure 4.7. It is important to note that in size-exclusion chromatography, the first moment for any polymer can be found using a universal calibration curve if K_x and a_x are available.

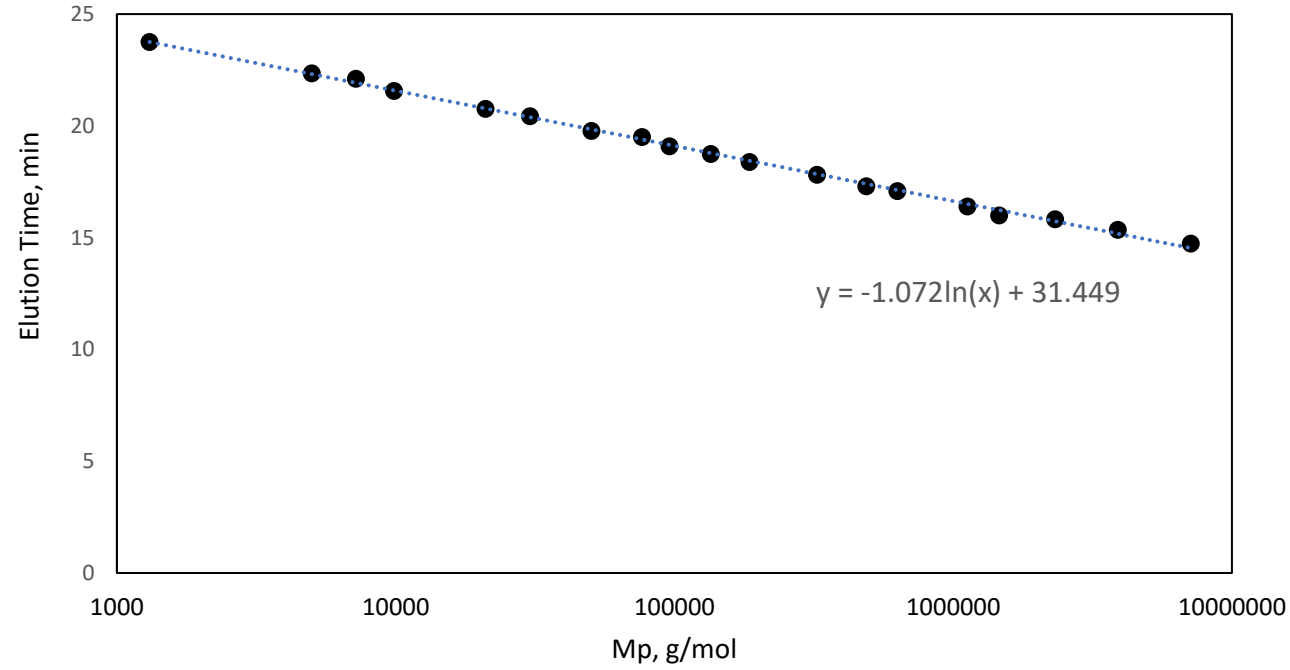

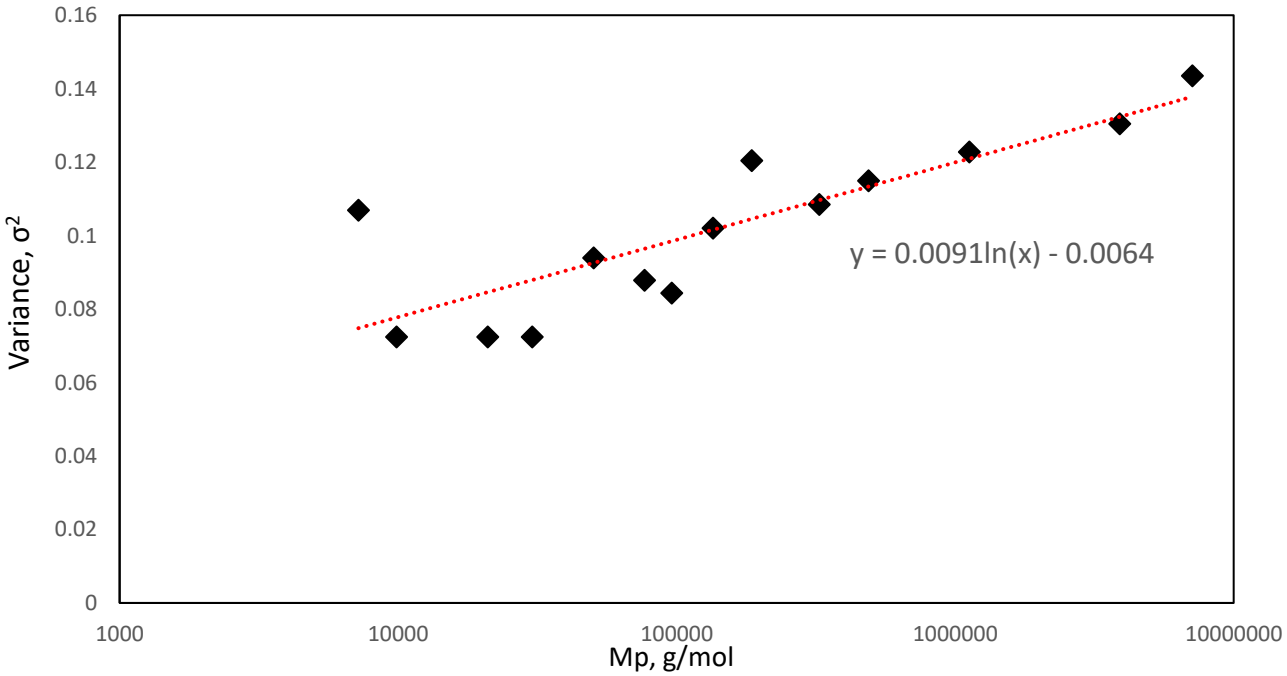

Figure 4.7: Elution time and variance as a function of peak molecular weight. The black circles and diamonds were obtained experimentally. The trends are represented by the dotted lines.

4.5 Simulation Comparison to Experimental Results

4.5.1 Predictive Model

Single Component System

Historical data was used in combination with immediate experimental results to test the proposed model. Each sample of polystyrene standard was prepared by measuring 6 to 8 mg of polystyrene into a 10 ml glass vial. A hand crimper was used to seal each vial with a rubber seal cap and then the vials were placed into the sample wells for injection into the SEC column.

Figure 4.8 compares experimental data and simulation results obtained from the Gaussian predictive model, calculated with the procedure outlined in Section 4.1 for several polystyrene standards. The trend line equations obtained from Figure 4.8 were used to estimate the first and second moments. A molecular weight interval dMW = 5 was used when splitting the Poisson distribution into several fractions, which was generated using a built-in function in Matlab®.

The experimental elution profiles closely resemble the results generated with the Gaussian distribution used in the predictive model. As the molecular weights of the polystyrene standards increase, so does their peak widths. As previously stated, the elution time of polystyrene standards is shorter for larger molecular weights, as expected. This is seen when comparing the peak times between each figure. For example, Figure 4.8a) shows the peak of PS1310 eluting from the column at approximately 24 minutes, while Figure 4.8f) shows that the peak of PS2320000 elutes sooner at approximately 15.6 minutes. Figure 4.8 shows that the predicted results agree well with the experimental data when comparing the elution time, peak width, and peak height.

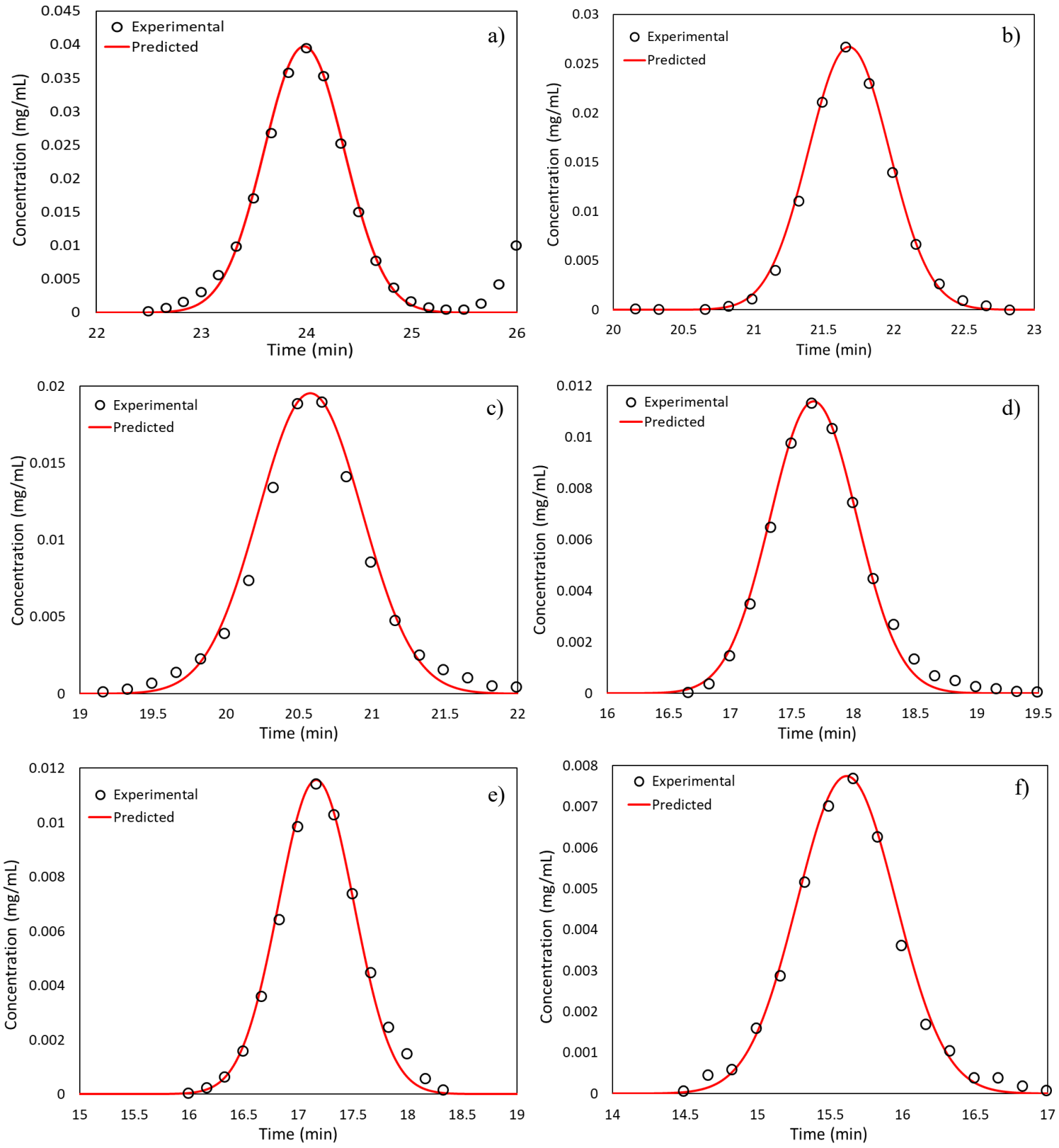

Figure 4.8: Experimental and predicted elution profiles for polystyrene standards: a) PS1310, b) PS9860, c) PS30300, d) PS325000, e) PS488000, and f) PS2320000.

Mixture System

Each mixture of polystyrene standards was prepared by measuring the amount specified in Table 4.4 into a 10 ml glass vial. Figure 4.9 compares experimental and Gaussian predicted elution profiles of multi-component mixtures of polystyrene standards. For each prediction, the elution profiles of the separate polystyrene standards where generated using the same procedure described in the previous section, and then added together to form a single elution profile. Table 4.4 shows the composition of each mixture simulated for Figures 4.9a-4.9d.

Even in the more complex three and four component systems, the model could predict the experimental elution profiles quite accurately using Gaussian distributions. This can be seen when comparing the elution times of the same standard between Figures 4.8 and 4.9. For example, PS325000 possesses the same peak elution time of 17.8 minutes in Figure 4.8d) and Figure 4.9b), while PS488000 exhibits an elution time of 17.3 minutes in Figure 4.8e) and Figure 4.9c). This also confirms that any interaction between solutes during the fractionation is negligible.

Table 4.4: Experimental mixture compositions used in Figures 4.9a-4.9d

Figure	PS	Mass (mg)	C_{inj} (mg/mL)
4.9a	7 200	8.1	0.0147
	76 600	8.0	0.0145
	1 124 000	4.5	0.0082
4.9b	5 000	6.7	0.0104
	135 000	5.5	0.0086
	325 000	5.3	0.0083
	1 460 000	3.1	0.0049
4.9c	30 300	8.1	0.0120
	488 000	4.7	0.0070
	1 124 000	6.5	0.0097
	7 100 000	4.0	0.0059
4.9d	13 000	6.5	0.0098
	186 000	4.6	0.0069
	630 000	5.2	0.0079
	3 900 000	3.7	0.0056

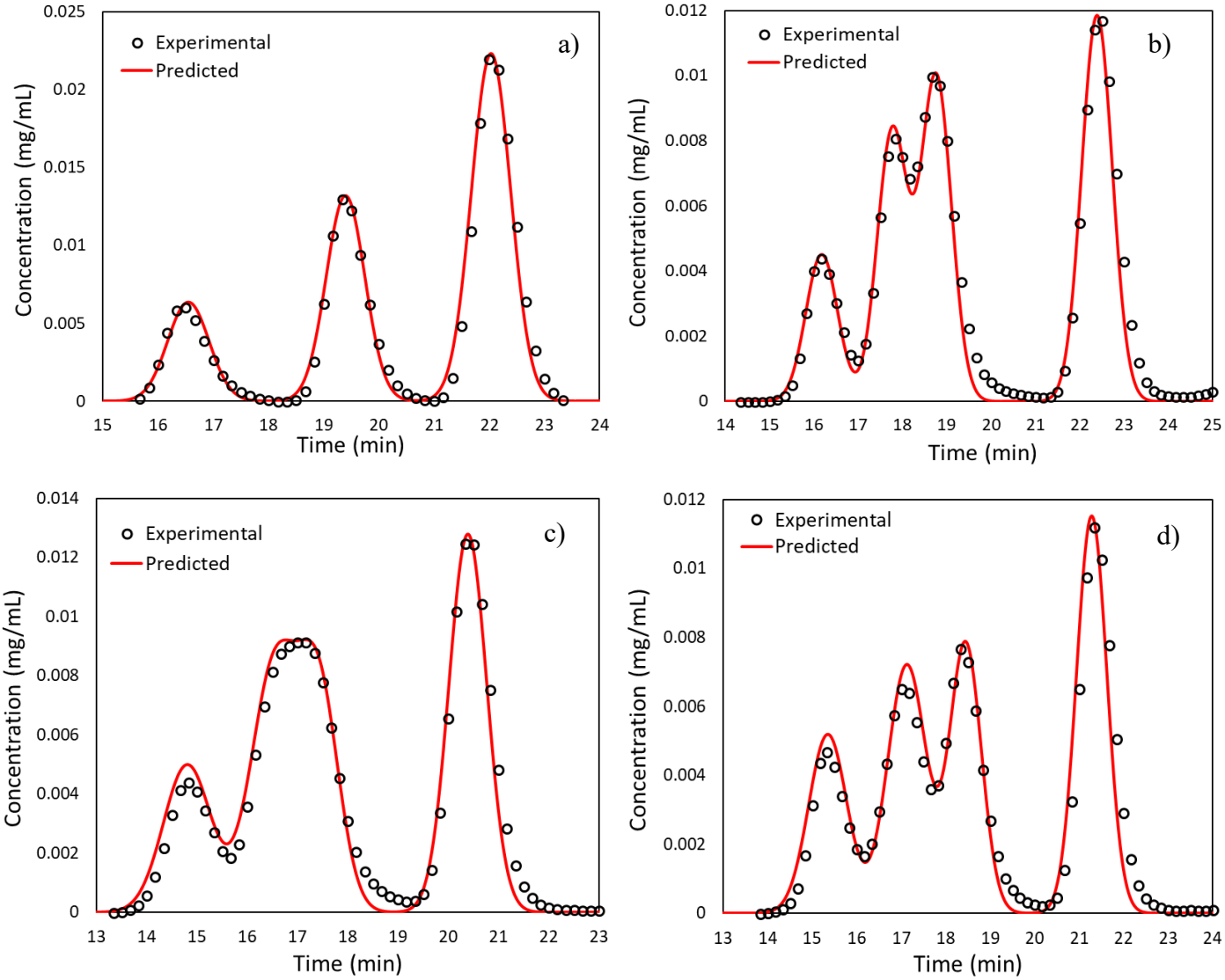

Figure 4.9: Experimental and predicted elution profiles of a mixture of polystyrene standards: a) PS7200, PS76000, PS1124000; b) PS5000, PS135000, PS325000, PS1460000; c) PS30300, PS488000, PS1124000, PS7100000; and d) PS13000, PS186000, PS630000, PS3900000.

4.5.2 Lumped Kinetic Rate Model

Single Component System

The experimental data used in this section was the same used in Section 4.5.1. Figure 4.10 compares experimental data and the results obtained from the rate model simulation for the same polystyrene standards presented in Section 4.4.1. Table 4.5 shows the physical parameters used to generate Figures 4.10a – 4.10f. The values of ε_p and D_b listed in Table 4.5 were calculated from Equations (4.3) and (4.2) respectively. Physical parameters including column length and diameter, flow rate, injection time, and bed porosity used are listed in Table 4.1. Also, the lumped mass transfer coefficient was $k_m = 1\ s^{-1}$ for all simulations.

Similar to the Gaussian-predictive model, the simulated results agree well with the experimental data when looking at the elution time, peak width, and peak height. From Figure 4.10, the agreement between the first moments of the experimental and rate model is acceptable. However, there are minor discrepancies between the peak shapes, especially when simulating polystyrene standards with higher molecular weights. One reason for the deviations of the model may be due numerical dispersion caused by the number of discretization points. Increasing the number of discretization points would result in a narrower peak as seen in Section 4.3.3.

Table 4.5: Values of physical parameters used in Figures 4.10a-4.10f.

Figure	PS, M_p	ε_p	$D_L \times 10^4$ (cm^2/s)	C_{inj} (mg/mL)
4.10a	1 310	0.38	4.11	2.31
4.10b	9 860	0.28	2.63	1.04
4.10c	30 300	0.24	3.81	1.04
4.10d	325 000	0.14	6.13	0.60
4.10e	488 000	0.12	6.94	0.71
4.10f	2 320 000	0.06	6.70	0.40

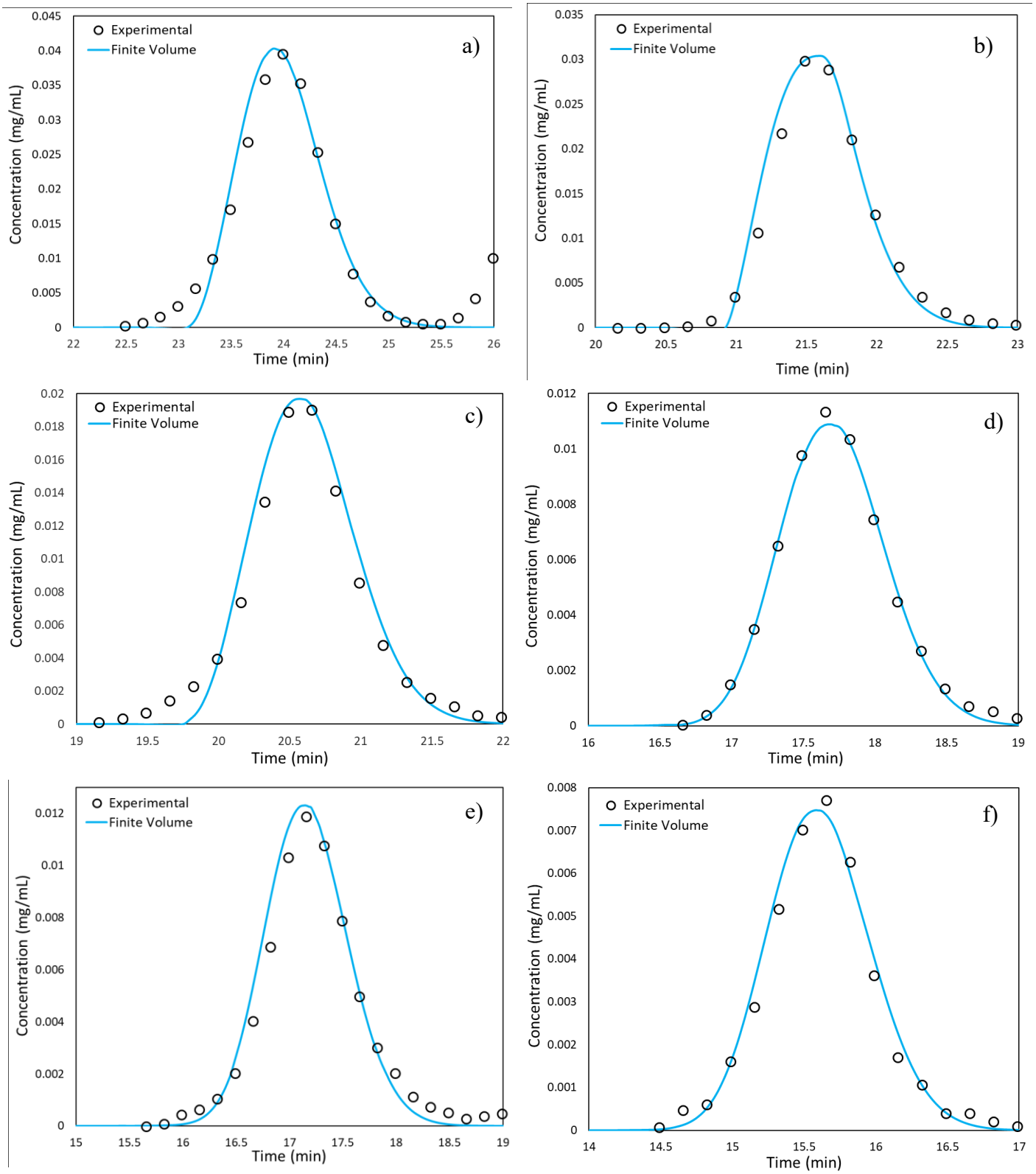

Figure 4.10: Experimental and predicted elution profiles for polystyrene standards: a) PS1310, b) PS9860, c) PS30300, d) PS325000, e) PS488000, and f) PS2320000.

Mixture System

The experimental data used in this section was the same used in Section 4.5.1. Comparisons between the model simulation and the experimental results of several mixtures of polystyrene standards are show in Figures 4.11a-4.11d. Table 4.6 shows the values used for Figures 4.11a – 4.11d. The values of ε_p and D_b listed in Table 4.5 were calculated from Equations (4.3) and (4.2), respectively. For each simulation, the elution profiles of separate polystyrene standards where generated and then combined to form a single chromatogram. The mixture compositions and physical parameters are shown in Table 4.6. The column length and diameter, flow rate, injection time, and bed porosity used are listed in Table 4.1. Also, the lumped mass transfer coefficient was $k_m = 1\ s^{-1}$ for all simulations.

Table 4.6: Physical parameters and experimental mixture compositions used in Figures 4.11a-4.11d.

Figure	PS, M_p	ε_p	$D_L \times 10^4$ (cm^2/s)	Mass (mg)	C_{inj} (mg/mL)
4.11a	7 200	0.31	2.51	8.1	0.0147
	76 600	0.20	3.75	8.0	0.0145
	1 124 000	0.08	8.20	4.5	0.0082
4.11b	5 000	0.32	3.62	6.7	0.0104
	135 000	0.17	5.80	5.5	0.0086
	325 000	0.14	6.13	5.3	0.0083
	1 460 000	0.07	5.85	3.1	0.0049
4.11c	30 300	0.24	3.81	8.1	0.0120
	488 000	0.12	6.94	4.7	0.0070
	1 124 000	0.08	8.20	6.5	0.0097
	7 100 000	0.02	17.0	4.0	0.0059
4.11d	13 000	0.28	2.71	6.5	0.0098
	186 000	0.16	5.43	4.6	0.0069
	630 000	0.11	9.61	5.2	0.0079
	3 900 000	0.04	10.3	3.7	0.0056

Figure 4.11 shows simulations and the experimental results agree well. Similar to the Gaussian-predictive model, the kinetic rate model is able to accurately calculate the peak width and elution time. It can be concluded that we can accurately model the size-exclusion chromatography process of a mixture of polystyrene standards.

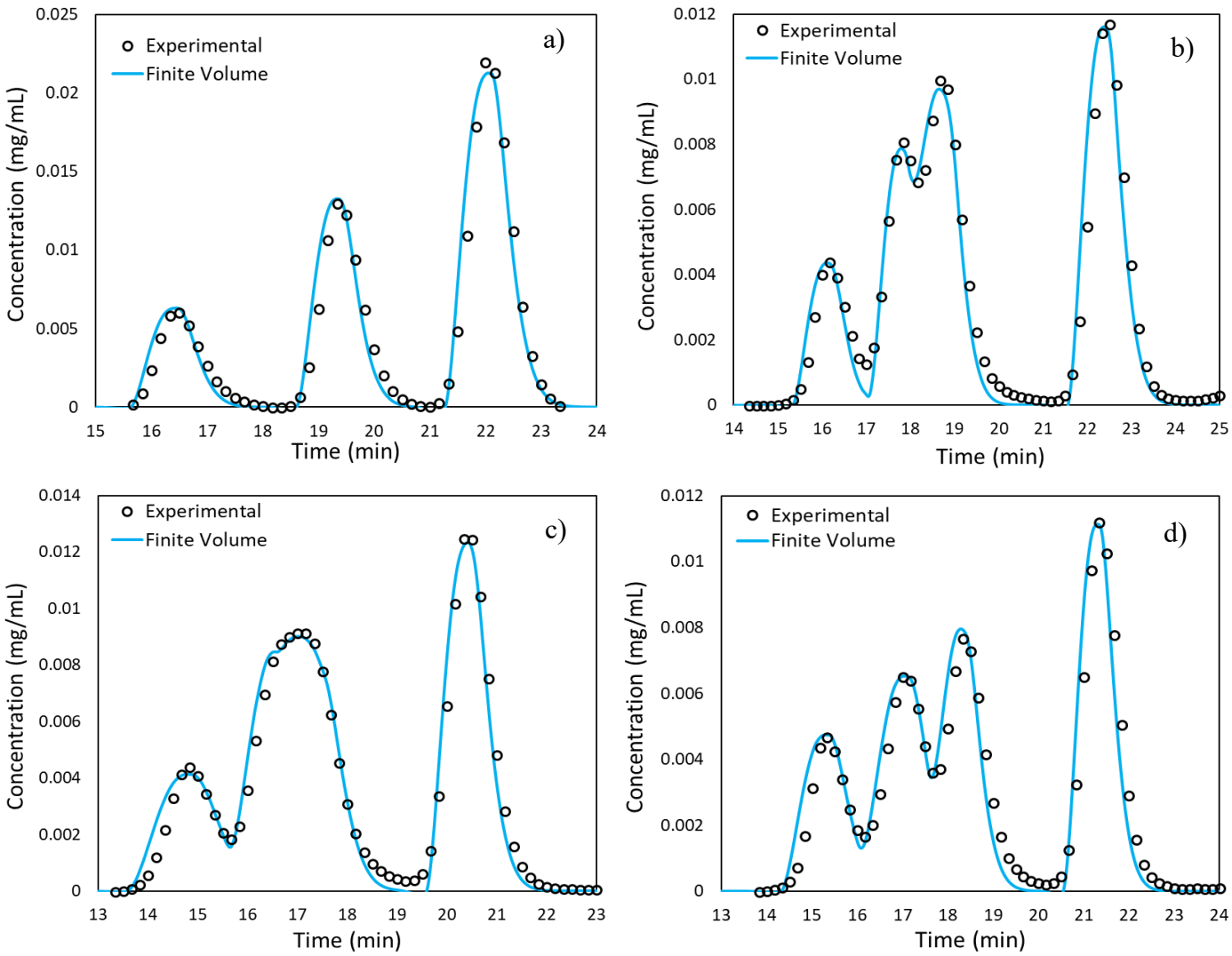

Figure 4.11: Experimental and simulated elution profiles of several mixtures of polystyrene standards: a) PS7200, PS76600, PS1124000; b) PS5000, PS135000, PS325000, PS1460000; c) PS30300, PS488000, PS1124000, PS7100000; and d) PS13000, PS186000, PS630000, PS3900000.

When comparing the Gaussian-predictive and the lumped kinetic rate models, while both agree well with the experimental results, the Gaussian approach seems to work as well as, if not better, than the finite element model for the set of samples analyze at the lab scale. However, this model does not consider the mass transfer resistances or the size of the column. The effect of mass transfer resistances on elution profiles become more prevalent as the diameter of the column increases, causing band broadening that could not be factored into the Gaussian-predictive model. This model also relies on predetermined trends relating the molecular weight to the first and second moments, which are easy to measure for polystyrene standards but become more difficult to obtain for more complex polymers possessing little historical data.

It is important to note that while the Gaussian-predictive and simulated results agree well with the experimental data in Figures 4.10 and 4.11, there are still some minor discrepancies between the elution times and peak shapes. Figure 4.12 compares the PDIs provided by the polymer manufacturer and the variances measured from the experimental and simulated data. The simulated values tend to predict broader peaks than the experimental results, especially with larger polystyrene standards. As it was shown previously in Figure 4.4, there is a significant effect that the number of discretization points has on the shape of the elution profiles. Increasing the number of discretization points used would decrease numerical dispersion generated from the model thus decreasing the variance of the simulated elution profiles.

Additionally, Figure 4.12 shows that the variances of the simulated and experimental data share a similar trend with the PDI, as the size in solution of the polystyrene standard increases. Therefore, band broadening caused by molar mass polydispersity produced by the polymerization mechanism can be disregarded to explain the discrepancies between the experimental and simulated results. Many peaks, even narrow standards, may deviate from non-Gaussian peak shapes due to band broadening effects, such as those discussed in Section 2.7.4.

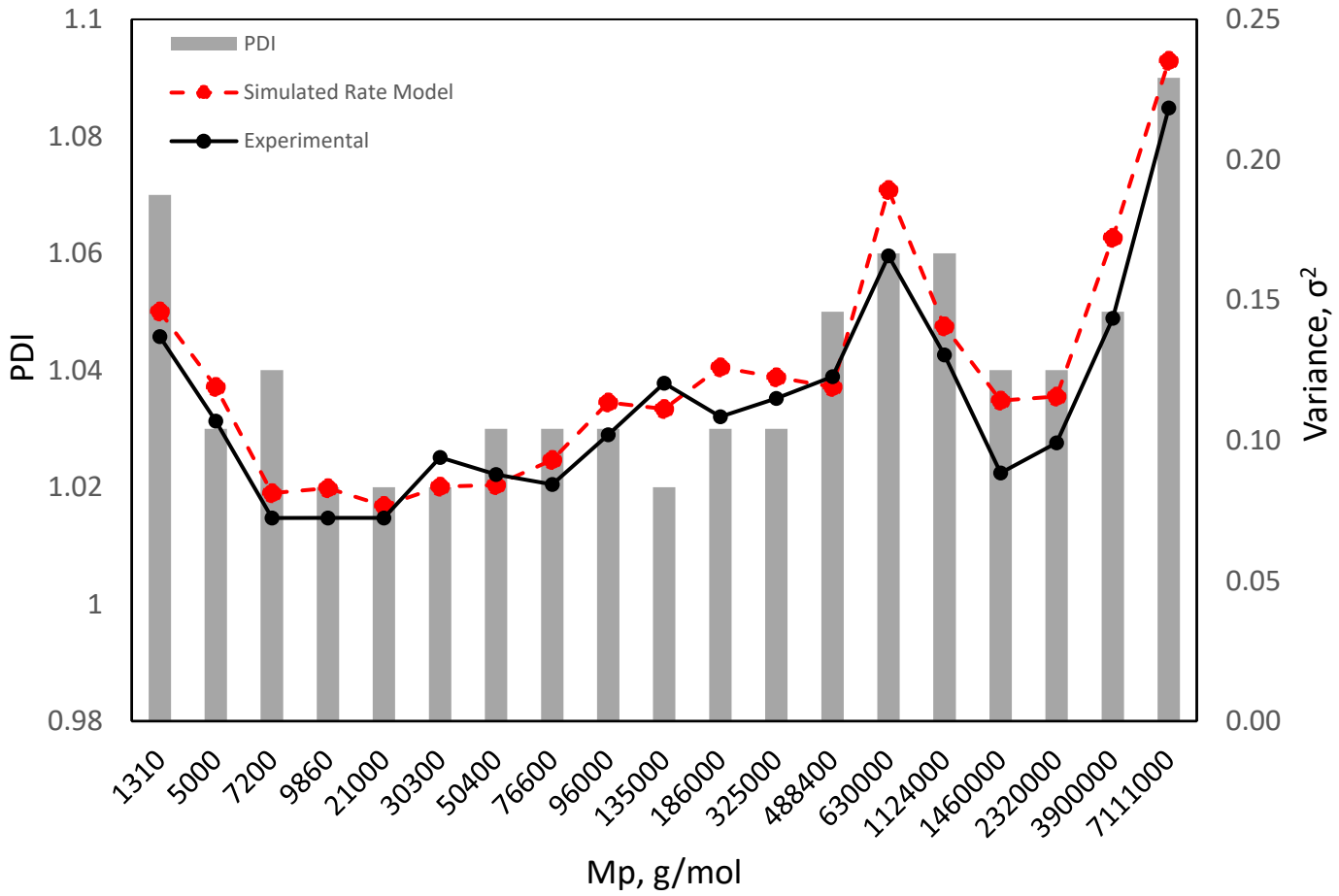

Figure 4.12 Comparison of simulated and experimental PDI and variances.

Chapter 5 Conclusion and Future Work

A predictive gaussian model and a kinetic lumped rate model were used to simulate the size-exclusion chromatography of polystyrene standards for the scale-up of SEC columns. The validity of the models was demonstrated using experimentally obtained model parameters.

For the kinetic rate model, mass transfer parameters were calculated from existing mass transfer correlations. Model predictions agreed well with the experimental results. However, minor differences between model predictions and experimental results were present, might be due to numerical dispersion or non-ideal packing of the SEC column.

Because size-exclusion chromatography separation only involves mass transfer interactions without adsorption, it is expected that the models can be used reliably for the purposes of scale-up, if there are no significant flow anomalies in the large columns.

A few lines for future research are proposed below:

1. The current investigation only considered the lumped kinetic model. It would be important to determine if the results simulated from a multicomponent general rate model would yield significantly more accurate results.
2. Other polymers were not investigated in this thesis. Using other types of polymers will help confirm the accuracy of the models presented.
3. Building a larger SEC column can help verify the accuracy of the models for the purposes of scale up since this study focused only lab scale SEC instrumentation.

Bibliography

[1] Ch. Dhéré, “Michael Tswett — le Créateur de l'Analyse Chromatographique par Adsorption; sa Vie, ses Travaux sur les Pigments Chlorophylliens.” Candollea (Genève) 10 (1943) pp: 23–73

[2] Guiochon G., Felinger A., Shirazi D.G., Katti A.M., Fundamentals of Preparative and Nonlinear Chromatography. Elsevier Inc., The Netherlands (2006)

[3] Guiochon G., Lin B., (2003) Modelling for Preparative Chromatography. Elsevier Science, California

[4] Striegel A., Kirkland J.J., Yau W.W., Bly D.D., Modern Size-Exclusion Liquid Chromatography. Wiley, New Jersey (2009)

[5] Moore J.C., Gel permeation chromatography I, new method for molecular weight distribution of high polymers, J. Polym. Sci., Pt. B2 (1964) pp: 835-843.

[6] Li Z., et al. Mathematical modeling and scale-up of size-exclusion chromatography, Biochemical Engineering Journal 2 (1998) pp: 145-155

[7] Agilent Technologies Inc., Gel Permeation Chromatography Basics and Beyond, https://www.agilent.com/cs/library/eseminars/public/Gel%20Permeation%20Chromatography%20Basics%20and%20Beyond.pdf (accessed May 20, 2018)

[8] Snyder L.R., Kirkland J.J., Dolan J.W., Introduction to modern liquid chromatography. Wiley, New York (2010)

[9] Carta G., Jungbauer A., Protein Chromatography Process Development and Scale-up [e-book]. Wiley-VCH (2010)

[10] Gu T., Mathematical Modeling and Scale-Up of Liquid Chromatography. Springer, Switzerland (2015)

[11] Rathore A.S., Velayhudan A., Scale-up and Optimization in Preparative Chromatography. Marcel Dekker, Inc., New York (2002)

[12] Dorsey J.G., Dill K.A., The molecular mechanism of retention in reversed-phase liquid chromatography, Chem. Rev., 89 (2), (1989) pp: 331–346

[13] Ladisch M.R., (2001) Bioseparations Engineering: Principles, Practice, and Economics. Wiley, New York

[14] Snyder L.R., Kirkland J.J., Glajch J.L., Practical HPLC Method Development. Wiley, New York (2012)

[15] Pfannkoch E., Lu K.C., Regnier F.E., Barth H.G., Characterization of Some Commercial High-Performance Size-Exclusion Chromatography Columns for Water-Soluble Polymers, J. Chrom. Sci., 18 (9), (1980) pp: 430–441

[16] Petro M., Svec F., Gitsov I., Fréchet J.M.J., Molded Monolithic Rod of Macroporous Poly(styrene-co-divinylbenzene) as a Separation Medium for HPLC of Synthetic Polymers: "On-Column" Precipitation−Redissolution Chromatography as an Alternative to Size Exclusion Chromatography of Styrene Oligomers and Polymers., Anal. Chem., 68 (2), (1996) pp: 315–321

[17] Gaborieau, M., Castignolles, P., Size-exclusion chromatography (SEC) of branched polymers and polysaccharides. Anal. Bioanal. Chem., 399, (2011) pp: 1413-1423

[18] Lafleur A.L., Nakagawa Y., Multimode size exclusion chromatography with poly(divinylbenzene)/N-methylpyrrolidinone for the characterization of coal-derived mixtures, Fuel, 68 (6), (1989) pp: 741-752

[19] Herod A. A., Shearman J., Lazaro M.J., Johnson B. R., Bartle K. D., Kandiyoti R., Effect of LiBr Addition to 1-Methyl-2-pyrrolidinone in the Size-Exclusion Chromatography of Coal-Derived Materials, Energy Fuels, 12 (1), (1998) pp: 174–182

[20] Hopia, A.I., Piironen, V.I., Koivistoinen, P.E. et al. Analysis of lipid classes by solid-phase extraction and high-performance size-exclusion chromatography, J. Am. Oil. Chem. Soc., 69, (1992) pp: 772-776

[21] Kawate, T., Gouaux E., Fluorescence-Detection Size-Exclusion Chromatography for Precrystallization Screening of Integral Membrane Proteins, Structure, 14 (4), (2006) pp: 673-681

[22] Wen J., Arakawa T., Philo J.S., Size-Exclusion Chromatography with On-Line Light-Scattering, Absorbance, and Refractive Index Detectors for Studying Proteins and Their Interactions, Anal. Biochem., 240 (2), (1996) pp: 155-166

[23] Uversky V.N., Use of fast protein size-exclusion liquid chromatography to study the unfolding of proteins which denature through the molten globule. Biochem., 32 (48), (1993) pp: 13288–13298

[24] Folta-Stogniew E., Williams K., Determination of molecular masses of proteins in solution: Implementation of an HPLC size exclusion chromatography and laser light scattering service in a core laboratory, J. Biomol. Tech., 10 (2), 1999 pp: 51–63.

[25] Giddings J. C., Dynamics of Chromatography, Part 1, Principles and Theory. Dekker, New York (1999)

[26] Trathnigg B., Size-exclusion Chromatography of Polymers, Encyclopedia of Analytical Chemistry, (2000) pp: 8008–8034

[27] Mori S., Barth H.G., Size Exclusion Chromatography. Springer-Verlag, Berlin (1999)

[28] Gucker F. T. and Seifert R. L. E, Physical Chemistry, W.W. Norton, New York (1966)

[29] Glockner G., Gradient HPLC and Chromatographic Cross-Fractionation. Springer, Berlin (1991)

[30] Dawkins J. V., Thermodynamic interpretation of polystyrene retention on crosslinked polystyrene gels in GPC with poor and theta solvents, J. Polym. Sci. A-2, 14 (569), (1976).

[31] Giddings J. C., Unified Separation Science, Wiley, New York (1991)

[32] Dubin P.L., Tecklenburg M. M., Size-exclusion chromatography of strong polyelectrolytes on porous glass columns, Anal. Chem., 57 (1), (1985) pp: 275–279

[33] Grubisic Z., Rempp P., Benoit H., A universal calibration for gel permeation chromatography, J. Polym. Sci. B., Polym. Letters 5, (1967) pp: 753-759.

[34] P. Debye, and A. M. Bueche, Intrinsic Viscosity, Diffusion, and Sedimentation Rate of Polymers in Solution, J. Chem. Phys., 16 (573), (1948)

[35] Kasaai M.R., Calculation of Mark–Houwink–Sakurada (MHS) equation viscometric constants for chitosan in any solvent–temperature system using experimental reported viscometric constants data., Carbohydr. Polym., 68, (2007) pp: 477–488

[36] Pelton R.H., A comparison of chain length distributions of polymers terminally and randomly anchored to a solid/solution interface, Colloids Surf., 40, (1989) pp: 43-48

[37] Chromacademy., The Theory of HPLC Chromatographic Parameters, http://www.chromacademy.com/lms/sco2/Theory_Of_HPLC_Chromatographic_Parameters.pdf (accessed June 2, 2018)

[38] Agilent Technologies Inc., HPLC Separation Fundamentals, https://www.agilent.com/cs/library/slidepresentation/public/HPLC%20Separation%20Fundamentals%20-%20011409.pdf (accessed May 20, 2018)

[39] Le Vent S., Simulation of chromatographic peaks by simple functions, Analytica Chimica Acta, 312 (3), (1995) pp: 263-270

[40] James A. T., Martin A. J. P., Gas- Liquid Partition Chromatography. A Technique for the Analysis of Volatile Materials, Analyst, 77 (915), (1952) pp: 915-932.

[41] Goyon A., Guillarme D., Fekete S., ., The importance of system band broadening in modern size exclusion chromatography, J. Pharm. Biomed. Anal., 135, (2017) pp: 50–60

[42] Xu J., Sun-Waterhouse D., Qiu C., Zhao M., Sun B., Lin L., Su G., Additional band broadening of peptides in the first size-exclusion chromatographic dimension of an automated stop-flow two-dimensional high-performance liquid chromatography, J. Chromatogr. A, 1521, (2017) pp: 80-89

[43] Wolpers A., Vana P., Chain-length-dependent impact of band broadening on the molar-mass determination of synthetic polymers via size-exclusion chromatography, J. Chromatogr. A, 1458, (2016) pp: 35-45

[44] Fekete S., Guillarme D., Influence of connection tubing in modern size exclusion chromatography and its impact on the characterization of mAbs. J. Pharm. Biomed. Anal., 149, (2018) pp: 22-32.

[45] Yau W.W., Brown R., Tyler P., Huang T., Cong R., Klinker C., Hazlitt L., A “Systematic Approach” to TD-GPC Data Processing with Band Broadening Correction, Macromol. Symp., 330, (2013) pp: 53–62

[46] Yau W.W., Characterizing Skewed Chromatographic Band Broadening, Anal. Chem., 49 (3), (1977) pp: 395-397

[47] Duerksen J. H., Comparison of Different Techniques of Correcting for Band Broadening in GPC, Sep. Sci., 5 (3), (1970) pp: 317-338,

[48] Piatkowski W., Antos D., Kaczmarski K., Modeling of preparative chromatography processes with slow intraparticle mass transport kinetics, J. Chromatogr. A, 988, (2003) pp: 219–231

[49] Stoisits R.F., Poehlein G.W., Vanderhoff J.W., Mathematical Modeling of Hydrodynamic Chromatography, J. Colloid Interface Sci., 57 (2), (1976)

[50] Kim H. H., Johnson A. F., Size-Exclusion Chromatography: Methodology and Characterization of Polymers and Related Materials, ACS Symp. Series, 245, (1984)

[51] Netopilik M., Relations between the separation coefficient, longitudinal displacement and peak broadening in size exclusion chromatography of macromolecules, J. Chromatogr. A, 978, (2002) pp: 109-117

[52] Saritha N. V., Madras G., Modeling the chromatographic response of inverse size-exclusion chromatography, Chem. Eng. Sci., 56, (2001) pp: 6511-6524

[53] Song M. S., Study on the concentration effects in size exclusion chromatography VII. A quantitative verification for the model theory of concentration and molecular mass dependences of hydrodynamic volumes for polydisperse polymers, J. Chromatogr. A, 961, (2001) pp: 155-170.

[54] Ruthven D.M., Principles of Adsorption and Adsorption Processes. Wiley, New York (1984)

[55] Edward F. Casassa, and Yukiko Tagami An Equilibrium Theory for Exclusion Chromatography of Branched and Linear Polymer Chains, Macromolecules, 2 (1), (1961) pp: 14–26

[56] Martin A. J. P., Synge R. L. M., A new form of chromatogram employing two liquid phases, Biochem. J., 35 (1358), (1941).

[57] Littlewood A. B., Gas Chromatography, 2nd ed., Academic Press, New York, (1970) Chap 5.

[58] Phillips C. S. G., Gas Chromatography, Academic Press, New York, (1956) pp: 95

[59] Gritti F., Guiochon G., Application of the General Height Equivalent to a Theoretical Plate Equation to Size Exclusion Chromatography. Study of the Mass Transfer of High-Molecular-Mass Compounds in Liquid Chromatography, Anal. Chem., 79 (8), (2007) pp: 3188–3198

[60] Glueckauf E., Coates J.I., Theory of chromatography. Part IV. The influence of incomplete equilibrium on the front boundary of chromatograms and on the effectiveness of separation, J. Chem. Soc., (1947) pp: 1315–1321

[61] Lin B., Golshan-Shirazi S., Ma Z., Guiochon G., Shock effects in nonlinear chromatography, Anal. Chem., 60, (1988) pp: 2647–2653

[62] Giddings J., Dynamic of Chromatography. Dekker, New York (1965)

[63] van Deemter J.J., Zuiderweg F.J., Klinkenberg A., Longitudinal diffusion and resistance to mass transfer as causes of nonideality in chromatography, Chem. Eng. Sci., 5, (1956) pp: 271-289

[64] Morbidelli M., Servida A., Storti G., Carra S., Simulation of multicomponent adsorption beds. Model analysis and numerical solution, Ind. Eng. Chem. Fundam., 21, (1982) pp: 132-131

[65] Rüdt M, Gillet F, Heege S, Hitzler J, Kalbfuss B, Guélat B., Combined Yamamoto approach for simultaneous estimation of adsorption isotherm and kinetic parameters in ion-exchange chromatography, J. Chromatogr. A, 1413, (2015) pp: 68-76

[66] Felinger A, Cavazzini A., Equivalence of the microscopic and macroscopic models of chromatography: stochastic-dispersive versus lumped kinetic model, J. Chromatogr. A, 1043 (2), (2004) pp: 149-157.

[67] Müller-Späth T., Ströhlein G., Aumann L., Kornmann H., Valax P., Delegrange L., Charbaut E., Baer G., Lamproye A., Jöhnck M., Schulte M., Morbidelli M., Model simulation and experimental verification of a cation-exchange IgG capture step in batch and continuous chromatography, J. Chromatogr. A, 1218 (31), (2011) pp: 5195-5204

[68] Foo K.Y., Hameed B.H., Insights into the modeling of adsorption isotherm systems, Chem. Eng. J., 156 (1), (2010) pp: 2-10

[69] Kovats E., in: Bruner F. (Ed.), The science of chromatography: lectures. Elsevier, The Netherlands, (1985) p.205

[70] Danckwerts P.V., Continuous flow systems. Distribution of residence times., Chem. Eng. Sci., 2 (1), (1952)

[71] Yu Q., Wang N.H.L., Computer simulations of the dynamics of multicomponent ion exchange and adsorption in fixed beds—gradient-directed moving finite element method, Comput. Chem. Eng., 13, (1989) pp: 915–926

[72] Gu T., Tsai G-J, Tsao G.T., New approach to a general nonlinear multicomponent chromatography model, AIChE J., 36, (1990) pp: 784–788.

[73] Gopinathan N., Fairweather M., Jia X., Computational modelling of packed bed systems, Comput. Aided Chem. Eng., 14, (2003) pp: 647-652

[74] Zelic B., Nesek B., Mathematical Modeling of Size Exclusion Chromatography, Eng. Life Sci., 6 (2), (2006) pp: 163-169

[75] de Klerk A., Voidage variation in packed beds at small column to particle diameter ratio, AIChE J., 49 (8), (2003) pp: 2022-2029